Available online at www.sciencedirect.com

ScienceDirect

Geochimica et Cosmochimica Acta 324 (2022) 262–279

Geochimica et Cosmochimica Acta

www.elsevier.com/locate/gca

Carbon and hydrogen isotopes of taraxerol in mangrove leaves and sediment cores: Implications for paleo-reconstructions

Ding He [a,b,*], S. Nemiah Ladd [c,1], Jiwoon Park [d], Julian P. Sachs [d], Bernd R.T. Simoneit [e], Joseph M. Smoak [f], Rudolf Jaffé [b]

[a] *Department of Ocean Science and Hong Kong Branch of the Southern Marine Science and Engineering Guangdong Laboratory (Guangzhou), The Hong Kong University of Science and Technology, Hong Kong, China*

[b] *Department of Chemistry and Biochemistry, and Southeast Environmental Research Center, Florida International University, Miami, FL 33199, USA*

[c] *Ecosystem Physiology, University of Freiburg, 79110 Freiburg, Germany*

[d] *School of Oceanography, University of Washington, Seattle, WA 98195, USA*

[e] *Department of Chemistry, College of Science, Oregon State University, Corvallis, OR 97331, USA*

[f] *School of Geosciences, University of South Florida, St. Petersburg, FL 33701, USA*

Received 6 September 2021; accepted in revised form 16 February 2022; Available online 23 February 2022

Abstract

Reconstructing past climate change in mangrove swamps contextualizes ongoing and future developments in these globally important ecosystems. Taraxerol, a well-recognized lipid biomarker for mangroves, is a promising target compound for calibration since it is relatively refractory and well preserved in sediments and since mangrove lipid δ^2H and $\delta^{13}C$ values have been shown to respond to salinity changes. Here we investigate the δ^2H and $\delta^{13}C$ values of taraxerol in leaves of two mangrove species (*Rhizophora mangle* and *Laguncularia racemosa*) and three dated mangrove cores along a spatial transect from the Shark River Estuary of South Florida, USA, to constrain its applicability for hydroclimate reconstructions. The net ^2H discrimination between surface water and taraxerol increased by 1.0‰ ppt^{-1} over a salinity range of 0.7–32 ppt for both *R. mangle* and *L. racemosa*. Although the $\delta^{13}C$ values of taraxerol showed a significant positive correlation with salinity in *L. racemosa*, the inverse trend was observed in *R. mangle*. The isotopic signature and spatial trends of taraxerol observed in mangrove leaves were well imprinted in mangrove surface sediments.

In addition, we further tested if the isotopic signal of taraxerol from mangrove leaves could be preserved in sediment cores on a time scale of ca. 300 yrs. No strong evidence of significant diagenetic alteration was observed for δ^2H values of taraxerol. In contrast, an increase up to ~1.1‰ was observed for $\delta^{13}C$, excluding the Suess effect. Considering the consistent salinity-dependent discrimination of ^2H to salinity, and no significant diagenetic alteration of taraxerol δ^2H values on centennial time scales, taraxerol H isotopes are a promising proxy for hydroclimate reconstruction in mangrove and mangrove-adjacent systems. However, the interpretation of $\delta^{13}C$ values of taraxerol should be treated with caution since its correlation with salinity may be species-specific and a slight diagenetic enrichment in ^{13}C may occur.

Keywords: Mangroves; Taraxerol; Hydrogen isotope; Carbon isotope; Early diagenesis; Paleoreconstruction

* Corresponding author.
E-mail address: dinghe@ust.hk (D. He).
[1] Department of Environmental Sciences, University of Basel, 4056 Basel, Switzerland.

https://doi.org/10.1016/j.gca.2022.02.018
0016-7037/

1. INTRODUCTION

Estuaries play an important role in depositing terrestrial organic matter that is transported to coastal oceans (Canuel et al., 2012). Although mangroves, which are halophilic trees or shrubs that grow widely in the intertidal zones in the subtropics and tropics, only constitute a small proportion of the estuarine environment by area, they are important carbon deposition ecosystems (Rivera-Monroy et al., 2011; Breithaupt et al., 2012), particularly in tropical and sub-tropical areas. Due to the extreme spatial and temporal gradients in salinity where mangroves grow, the plant species diversity in mangrove swamps is usually low (Koch et al., 2003; Versteegh et al., 2004). In this regard, the sedimentary organic matter in mangrove habitats is predominantly derived from mangroves, and about a third of organic matter in subtropical and tropical coastal sediments is estimated to originate from mangrove leaf litter (Jennerjahn and Ittekkot, 2002; Giri et al., 2011; Alongi and Mukhopadhyay, 2015). Since plants such as mangroves respond biochemically to environmental changes and stressors, such conditions are likely to be imprinted in their molecular and isotopic character. As such, mangrove habitats have been reported to serve as ideal ecosystems for elucidating paleoclimate trends in tropical/subtropical areas (Koch et al., 2003; Ladd and Sachs, 2012; Nelson and Sachs, 2016). It is promising to use source-specific biomarkers for paleoreconstructions in mangrove soils (Koch et al., 2003; Versteegh et al., 2004), and carbon and hydrogen isotopes (δ^2H and $\delta^{13}C$ values) of specific lipid biomarkers have successfully been applied in paleoclimate reconstructions (e.g., Sachse et al., 2012; Diefendorf and Freimuth, 2017). However, the application of leaf wax δ^2H (δ^2H_{lipid}) values as a precipitation proxy in coastal tropical and subtropical regions can be complicated by the significant influence of salinity on hydrogen isotope fractionation in halophilic plant leaf waxes (Romero and Feakins, 2011; Ladd and Sachs, 2012, 2015a, b, 2017). Similarly, leaf wax $\delta^{13}C$ values can also be affected by salinity stress-related water availability and subsequent biochemical responses (e.g., Ladd and Sachs, 2013; He et al., 2021). Therefore, some significant challenges remain in this field.

There have been a growing number of studies assessing how $\delta^{13}C$ and δ^2H values of mangrove leaf wax *n*-alkane and other lipid compounds respond to salinity increase either along a spatial transect within a single site, with time-series observations, and in lab culture experiments (Ladd and Sachs, 2012, 2013, 2015a, b, 2017; He et al., 2017, 2020; Park et al., 2019). These studies have shown that: (a) $^2H/^1H$ fractionation between surface water and lipids ($\alpha^2H_{lipid\text{-}sw} = (1000 + \delta^2H_{lipid})/(1000 + \delta^2H_{surface\ water}$) of mangroves increases with salinity, resulting in lower δ^2H_{lipid} values at high salinity in both Indo-West Pacific and Americas-East Atlantic mangroves (He et al., 2017); (b) although net $^2H/^1H$ fractionation for *n*-C_{31}-alkane increased by 0.8‰, 1.4‰, and 1.8‰/ppt in *Rhizophora mangle*, *Avicennia germinans* and *Laguncularia. racemosa*, respectively, no statistically significant difference in the sensitivity of $\alpha^2H_{C31\ n\text{-}alkane\text{-}sw}$ to salinity was observed in four *Rhizophora* species from both Indo-West Pacific and America-East Atlantic regions, making sedimentary *Rhizophora* lipids a promising target for paleohydroclimatic reconstruction (He et al., 2017); in addition, some studies have investigated lipid compounds other than *n*-alkanes from mangroves, including stigmasterol and β-sitosterol (Ladd and Sachs, 2015a), lupeol (Ladd and Sachs, 2017), and fatty acids (Park et al., 2019), and observed negative correlations between salinity and $\alpha^2H_{lipid\text{-}sw}$; (c) both positive and negative correlations between salinity and leaf wax *n*-alkane $\delta^{13}C$ values were observed across mangrove species (Ladd and Sachs, 2013; Park et al., 2019; He et al., 2021), suggesting factors other than salinity, such as differences in photosynthetic activity, growth rate, and nutrient supply, likely affect carbon isotopic fractionation in mangroves.

Although *n*-alkanes are resistant to degradation and thus widely detected in geological records, they can be derived from both terrestrial and aquatic sources (Bianchi and Canuel, 2011). Even when focusing on long-chain *n*-alkanes, they could be derived from diverse origins in mangrove systems including from terrestrial plants associated with the mangrove ecosystem and adjacent wetlands, seagrass beds, and others (Ladygina et al., 2006; Nelson et al., 2018; He et al., 2020; Chen et al., 2021). Similar ambiguity of source-tracing also exists for most sterols and fatty acids (e.g., Bianchi and Canuel, 2011). For instance, numerous terrestrial plants can produce considerable amounts of stigmasterol, β-sitosterol, lupeol and long-chain fatty acids (e.g., Bianchi and Canuel, 2011 and references therein). Although most commonly mangrove ecosystems are dominated by organic matter derived from their leaf litter, the empirical correlations between salinity and mangrove leaf wax *n*-alkane fractionation factors may not be well suited for all paleoenvironmental reconstructions, especially when mangrove-influenced coastal sediments receive organic matter (OM) input from non-mangrove plants (Xu and Jaffé, 2007), or where a significant ecological shift from other species (i.e., salt marshes) to mangroves and vice versa has occurred (e.g., Vaughn et al., 2020). For example, a recent study suggested that mangroves complicate hydrological reconstructions due to the input of long-chain *n*-alkyl lipids from terrestrial plant waxes, although such a complication can be reasonably corrected via parallel analysis of pollen data (Tamalavage et al., 2020).

In contrast to *n*-alkanes, fatty acids, most sterols and triterpenoids, taraxerol, a pentacyclic triterpenoid, has the potential to be used as a source specific molecular marker for mangroves since it occurs in extremely high abundance in certain mangrove leaves, especially the *Rhizophora* genus (Killops and Frewin, 1994; Dodd et al., 1998; Chu et al., 2020), and to a lesser extent in *A. germinans* (Koch et al., 2005) and *L. racemosa* (He et al., 2018b). However, it has also been detected in lower amounts in some peat-forming higher plants that potentially can be associated with fringe mangrove ecosystems (e.g., Pancost et al., 2002), as well as in a wide diversity of non-mangrove vascular plants (Sharma and Zafar, 2015). Moreover, taraxerol is routinely detected in mangrove estuary suspended particulates (He et al., 2014; Xu and Jaffé, 2007), surface sediments (Volkman et al., 1987; Koch et al., 2003, 2011; Xu et al.,

2006; Xu and Jaffé, 2007; Chu et al., 2020), and estuarine and marine sediment cores (Koch et al., 2003; Versteegh et al., 2004; Scourse et al., 2005; Xu et al., 2007; He et al., 2018b) spanning time scales from 10^2-10^6 years (up to 1250 kyr B.P.).

Despite its wide occurrence and reports in geological studies, very few studies have examined the isotopic signature of taraxerol. Lockheart et al. (1997) reported the $\delta^{13}C$ value of taraxerol from the leaves of modern angiosperms (*Quercus robur*) and found it was enriched in ^{13}C compared to long-chain *n*-alkyl lipids, while Sauer et al. (2001) reported δ^2H values of taraxerol in lake sediments and found that it was more depleted in ^2H than the long-chain *n*-alkyl lipids. Recent studies investigated the δ^2H values of taraxerol in mangrove leaves (Ladd and Sachs, 2015a, b), and found significant negative correlations between salinity and $\alpha^2H_{taraxerol\text{-}sw}$ for *Rhizophora* mangroves. This relationship allows paleo-precipitation and salinity to be reconstructed when taraxerol δ^2H values are paired with those of dinosterol, a diatom biomarker, (Nelson and Sachs, 2016). However, the $\delta^{13}C$ values of taraxerol from mangrove ecosystems remain relatively unexplored. Moreover, the combination of δ^2H and $\delta^{13}C$ values of taraxerol in mangrove sediment cores has never been investigated.

Although pentacyclic triterpenoids (including taraxerol) have been suggested to show high stability during early diagenesis (Hernes et al., 2001; Koch et al., 2003), widespread diagenetic degradation products from taraxerol were recently reported in mangrove surface sediments (He et al., 2018b). Moreover, the degradation of taraxerol through ring-A opening was reported to occur in mangrove leaves prior to leaf senescence (Simoneit et al., 2009; He et al., 2018b). Whether diagenetic alteration of taraxerol causes fractionation of C and H isotope needs to be evaluated to better constrain its applicability for paleoenvironmental reconstructions (Freeman et al., 1994; Sessions, 2016). Although there are no direct investigations of the paired C and H isotopic composition of taraxerol and its diagenetic products, a pioneering study by Freeman et al. (1994) suggested that the aromatization of pentacyclic triterpenes has little effect on their $\delta^{13}C$ values, but the impact of diagenesis on δ^2H values remains unknown. Within the marsh grass (*Spartina alterniflora*), the δ^2H values of pentacyclic triterpenones, early diagenetic (loss of hydrogen atoms) products of triterpenols, were up to 29‰ higher than those of pentacyclic triterpenols (Sessions et al., 1999). Chikaraishi and Naraoka (2005) investigated $\delta^{13}C$ and δ^2H values of various sterols and major fatty acids in the sediments of Lake Haruna, Japan. They found that although concentrations of lipid biomarkers generally decreased with depth in the sediment, the isotopic signatures of these biomarkers resisted diagenetic alteration, supporting the use of their isotopic compositions for paleoclimatic reconstructions using lake sediment cores. A later study by Li et al. (2009) investigated the δ^2H values of several types of compounds in typical estuarine and coastal environments in the Santa Barbara Basin. They found that neither anaerobic nor aerobic degradation of lipids imparts a measurable change in their hydrogen isotopic composition (Li et al., 2009). Yet these studies did not specifically target pentacyclic triterpenoids. Schaeffer et al. (2019) found that the $\delta^{13}C$ values of both di- and triterpenes were not significantly affected by progressive aromatization, whereas a significant increase of δ^2H values by up to 86‰ for diterpenoids related to abietic acid was observed with ongoing aromatization. Considering the well-constrained mangrove leaf source of taraxerol in tropical and subtropical coastal environments it is crucial to get a better understanding of its isotopic compositions ($\delta^{13}C$ and δ^2H) and the factors that affect them.

In this context, by sampling across mangrove species, spatial transects, and sediment cores, we aim to further evaluate the use of taraxerol as a paleoclimatic proxy in tropical/subtropical environments. Specifically, we investigated (i) $\delta^{13}C$ and δ^2H values of taraxerol in two mangrove species (*R. mangle* and *L. racemosa*) along a spatial transect from freshwater to seawater in the Shark River Estuary (SRE), Florida, USA, and (ii) $\delta^{13}C$ and δ^2H values of taraxerol and its dominant diagenetic products in three spatially distributed mangrove cores along the estuary (aged *ca.* 300 years). The main objective of this study was to determine whether there is a uniform response of C and H isotopic values of taraxerol to salinity and whether the isotopic signatures of taraxerol in sediments are preserved during deposition on centennial scales. In addition, the isotopic values of a long chain *n*-alkane (*n*-C_{31}-alkane) from mangrove leaves and sediments were obtained to compare with taraxerol. The ultimate goal of this study is to aid in establishing δ^2H and $\delta^{13}C$ values of taraxerol as paleoenvironmental indicators.

2. MATERIALS AND METHODS

2.1. Sampling

2.1.1. Mangrove leaves

The SRE is a mangrove-dominated estuary in the southwest region of the Florida Everglades, USA (Fig. 1), characterized by semi-diurnal tides with a mean amplitude of 1.1 m (Wanless et al., 1994). The dominant plant species in the SRE are mangroves, ranging in height between 5 and 13 m (Rivera-Monroy et al., 2011; Castañeda-Moya et al., 2013). Salinity and nutrient (phosphorus) levels increase along the estuary from site 1 to site 13 (Table S1). The sites also differ in the stature of the mangrove forests, with the downstream sites (8 to 13) having large trees, middle sites (5 to 7) having trees of intermediate height, and upstream sites (1 to 4) having mangroves described as low or dwarf in stature (Rivera-Monroy et al., 2011).

Mature leaves from *L. racemosa* and *R. mangle* were collected by hand along the estuary in March 2013 (Fig. 1). Multiple leaves were randomly collected from the sunny side of each mature mangrove tree (similar height) and immediately placed in plastic Ziploc bags and stored on ice. At each site, surface water salinity was measured (ca. 10 cm below surface) adjacent to the sampled tree three times to calculate the average salinity (Table S1). A linear regression of salinity on distance to the Shark River mouth

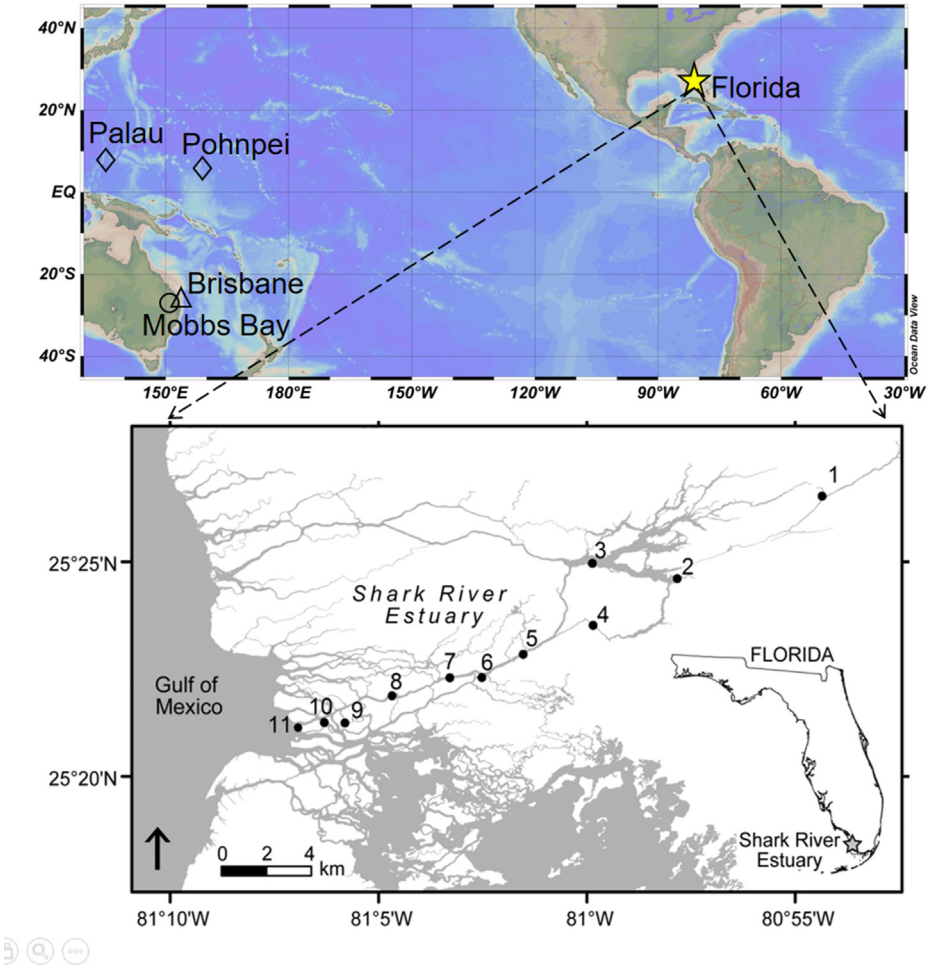

Fig. 1. Map of the Shark River estuary. Sampling sites are marked with bold numbers from 1-11. Detailed sampling information is also shown in Table S1. Note: data from Palau and Pohnpei are detailed in Ladd and Sachs (2015a, 2017); Brisbane in Ladd and Sachs (2012); Mobbs Bay in Ladd and Sachs (2015b).

yielded the equation: Salinity = −1.3949× (km of distance) + 31.745; R^2 0.97 (He et al., 2017). This equation was used to derive salinity so as to minimize the bias in measurements that occurred at various times throughout the tidal cycle.

2.1.2. Surface sediments and sediment cores

Three estuarine sites (sites 2, 5, and 8) from the upper, middle, and downstream sections of the SRE were selected for sediment coring (Fig. 1). Each of these sites was previously established by the Florida Coastal Everglades Long Term Ecological Research program (FCE-LTER; www.fcelter.fiu.edu). All sites are characterized as having peat soils with seasonally driven freshwater inputs and tidally driven seawater inputs. Sediment cores were collected from these three sites in year 2005 with a push corer (50 cm × 10 cm i.d.) that was manually pushed into the sediments. The cores were extruded in the field and cut into 5 cm sections, wrapped in pre-combusted aluminum foil, and placed into Ziploc bags that were stored on ice for transport to the laboratory where they were stored at −20 °C. Frozen samples were freeze-dried and then sieved through a Fisher Scientific 35 mesh (500 μm) sieve to remove coarse materials such as large roots and woody debris. The sieved freeze-dried samples were used for further bulk parameters and biomarker analysis.

Additional sediment cores from the same sites 2, 5, and 8 were sampled and used for dating, as reported in Smoak et al. (2013) and Breithaupt et al. (2014, 2017). In particular, freeze dried and ground sediments were packed and sealed in gamma tubes. Radiometric dating was achieved by measuring ^{210}Pb via gamma spectrometry (Smoak et al., 2013; Breithaupt et al., 2014). Because our study sites have been subject to hurricane activity, which would contribute a source of marine sediment deposition, the sediment accumulation rate has been calculated following the Constant Rate of Supply (CRS) model (Breithaupt et al., 2017). Since ^{210}Pb is a radionuclide with a half-life of 22.3 years, it is well suited to the centennial timescale. Based on the accumulation rates obtained previously (Breithaupt et al., 2017), we estimated the ages of cores 2, 5, and 8. In particular, we picked the deepest age which was reliable

(age error less than 15 years) for each core and took that age plus how long it would have taken given the rate in that interval to have accreted from the given depth (35 cm for core 2, and 40 cm for cores 5 and 8). Although the deepest age for each core is roughly estimated based on extrapolated ^{210}Pb age models and thus is not quantitatively assessed, all cores should reasonably cover > 150 years (with the deepest age came out around 185 to 228 years; Table S2).

2.2. Bulk parameter analyses

The bulk parameters of percent organic carbon (%OC) and C/N ratio (ratio of %OC over %TN) were measured in the SRE sediments. To eliminate possible interference due to inorganic carbon in the form of $CaCO_3$, %OC analyses on sediment samples were performed after treatment with 1 N HCl that was added dropwise until the cessation of bubbling. The acidified soils were allowed to sit overnight at room temperature, then neutralized with deionized water, frozen, and freeze-dried for analysis. The %OC and %TN were determined on a FLASH2000 Organic Elemental Analyzer with a combustion temperature of 1020 ℃.

The bulk $\delta^{13}C$ values of mangrove leaves and sediments were obtained using a FLASH2000 Organic Elemental Analyzer coupled to a Finnigan MAT delta Plus V mass spectrometer. Carbonate was removed from sediments as described above. Samples were measured in duplicate and mean values are reported. A reference standard material (glycine) was analyzed every five measurements, with the standard deviation of ± 0.2‰ (n = 24).

2.3. Biomarker analyses

Freeze-dried plant tissues and sub-samples of the sieved fine fractions (<500 μm) were Soxhlet extracted using dichloromethane for 24 hours. An excess of activated copper was added (only for the sediment extraction) to the receiving flask to remove elemental sulfur. Total extracts were saponified with 1.0 N KOH and separated into neutral and acid fractions. Acid fractions were recovered through acidification (pH < 2) using concentrated HCl followed by extraction with dichloromethane. Anhydrous Na_2SO_4 was added to remove residual water. The acid and neutral fractions were concentrated using a rotary evaporator and the solvent of the neutral fraction was exchanged with hexane before being further fractionated into eight fractions by adsorption column chromatography utilizing silica gel (7.0 g of silica gel, 5% deactivated by deionized H_2O, 100–200 mesh, Fisher Scientific). The aliphatic hydrocarbons were eluted with hexane, aromatics with hexane: toluene (3:1), ketones with hexane: ethyl acetate (9:1), alcohols with hexane: ethyl acetate (17:3) and the sterol fraction was eluted with hexane: ethyl acetate (4:1). The sterol fractions were derivatized with bis(trimethylsilyl)trifluoroaceta mide (BSTFA) before GC/MS analysis. Acid and neutral fractions were analyzed by capillary GC/MS on a HP 6890 GC interfaced to a HP 5973 quadrupole mass spectrometer. A 5% phenylmethylsilicone bonded phase (DB-5MS; Agilent) fused silica capillary column (30 m × 0.25 mm i.d. × 0.25 μm film thickness) was used for separations. For the analysis of the acid, aliphatic, and ketone fractions the GC oven was temperature programmed as follows: the initial temperature was 40 ℃ (held for 1 min), then ramped at a rate of 6 ℃/min to a final temperature of 300 ℃ (held for 20 min). For the analysis of the aromatic, alcohol, and sterol fractions the GC oven was temperature programmed as follows: the initial temperature was 60 ℃ (held for 1 min), ramped at a rate of 6 ℃/min to 180 ℃, and then ramped at a rate of 2.5 ℃/min to a final temperature of 315 ℃ (held for 15 min). The carrier gas (He) pressure was set at 10.74 psi, the transfer line temperature was 280 ℃, and the split/splitless injector was operated in splitless mode and set at 280 ℃.

2.4. Compound specific carbon and hydrogen isotope analyses

Compound-specific $\delta^{13}C$ values were obtained by gas chromatography-isotope ratio mass spectrometry (GC-IRMS), using an HP 6890 GC equipped with a DB-5 fused silica capillary column, a combustion interface (Finnigan GC combustion IV), and a Finnigan MAT delta Plus V mass spectrometer, following a previously published procedure (He et al., 2020). Briefly, three external standard mixtures containing *n*-heptadecane and squalane at different concentrations, with known $\delta^{13}C$ values of −21.3‰ and −29.5‰, respectively, were used to check instrument performance during the entire analysis period and for correction purposes. For the $\delta^{13}C$ measurement, $\delta^{13}C$ values are given in per mil (‰) notation relative to the Vienna Peedee Belemnite (VPDB) standard. Samples were analyzed at least two times, and the mean values are reported. Standard deviations of triplicate injections were always < 0.4‰. Precision for *n*-alkane carbon isotope determinations was ± 0.3‰ as determined by a co-injected secondary standard (squalane, −29.5‰). Correction for C added by derivatization of taraxerol by bis-(trimethylsilyl)-trifluoroa cetamide (BSTFA) was made by way of mass balance.

Compound-specific $\delta^{2}H$ values of individual *n*-alkanes and taraxerol were measured using a GC/Pyrolysis/IRMS system consisting of a HP 6890 GC connected to a Finnigan MAT Delta V mass spectrometer. The pyrolysis temperature was set at 1440 ℃ in a micro volume ceramic tube. Helium was used as carrier gas at 1.6 mL min^{-1}. Calibrated methyl palmitate (−255‰) and squalane (−107‰) mixtures with different concentrations were used as external standards. External standard calibration was performed after every four sample measurements. The F8 standard (obtained from Indiana University, Bloomington, USA) was analyzed at least every 6 samples, and had a measured accuracy of ± 3‰. The H_3^+ factor was measured daily before sample analysis and averaged 4.9 ± 0.1 during this study. $\delta^{2}H$ values were all normalized to the VSMOW (Vienna Standard Mean Ocean Water) scale by the nearest two F8 standards, and the internal co-injected squalane for each sample if necessary. Samples were analyzed at least two times and the mean values are reported. Standard deviations of triplicate injections were always < 4‰. The precision was assessed by the secondary reference material: the methyl palmitate and squalane mixed standards, and the

standard deviations were 3‰ and 3‰ for methyl palmitate and squalane, respectively, across the course of analyses. Correction for H added by derivatization of taraxerol by BSTFA was made by way of mass balance.

All derivatization was performed using the same batch of BSTFA, for which the δ^2H and $\delta^{13}C$ values were measured using calibrated standards (squalene and methyl palmitate) and TC/EA-IR-MS. δ^2H and $\delta^{13}C$ values of derivatized taraxerol were corrected for the added trimethylsilyl group by mass balance for the contribution of carbon and hydrogen added during derivatization (Rieley, 1994). The correction equations are listed as follows:

$$\delta^{13}C_{taraxerol} = (N_{Der}\delta^{13}C_{Der} - N_{BSTFA}\delta^{13}C_{BSTFA})/N_{taraxerol}$$

$$\delta^{2}H_{taraxerol} = (N_{Der}\delta^{2}H_{Der} - N_{BSTFA}\delta^{2}H_{BSTFA})/N_{taraxerol}$$

where N is the number of C or H atoms of the derivative (N_{Der}), the derivatization reagent (N_{BSTFA}), and the original taraxerol molecule ($N_{taraxerol}$).

The total uncertainty of $\delta^{13}C$ and δ^2H in the derivatized samples is ±0.5‰ and ±6‰, respectively, based on the sum of squares from precision in sample measurements and precision in the TMS carbon and hydrogen.

2.5. Estimation of surface water δ^2H values

Surface water δ^2H values are an important factor affecting the δ^2H values of mangrove leaf lipids, as observed in previous studies (Ladd and Sachs, 2015a, b, 2017). Although leaf wax formation is limited to the brief period of spring leaf emergence in deciduous plants (e.g., Tipple et al., 2013; Newberry et al., 2015), it may last for longer time scales (weeks to months, Jetter et al., 2006). This is likely the case for Florida mangroves, considering the leaf lifetimes are longer than 60 and 111 days in *L. racemosa* and *R. mangle*, respectively (Suárez, 2003). In contrast, precipitation water δ^2H values fluctuate on much shorter time scales (hours to days) in coastal ecosystems such as the Everglades (Price et al., 2008). Moreover, given the spatiotemporal variation in leaf water isotopic composition, measured bulk leaf water may not relate to the substrate used for the synthesis of leaf waxes. Therefore, we consider it appropriate to use averaged annual surface water δ^2H values rather than a single precipitation δ^2H value at the time of leaf collection to compare the net fractionation difference within and between species along the spatial transect.

The estimation of surface water δ^2H values has been documented previously (He et al., 2017). The weighted average δ^2H value (n = 43) of surface freshwater is −12.2‰ (Price et al., 2008). Surface seawater in the Gulf of Mexico has an average δ^2H value of 15‰ (Sternberg and Swart, 1987). Then the δ^2H value of surface water at each sampling location was estimated from measured salinity and referred to as "modeled surface water δ^2H values", assuming conservative mixing between average freshwater and Gulf of Mexico along the SRE (He et al., 2017), as observed in spatiotemporal investigations of mangrove ecosystems (Ladd and Sachs, 2012, 2015a, 2017). The corresponding mixing line is: modeled surface water δ^2H value per mil = (15 + 12.2)/(32–0.7) × salinity-12.2.

2.6. Statistical analyses

The Student t-test was conducted on R3.2.1 (R Core Team 2015) to compare among different groups of samples (e.g., *R. mangle* vs. *L. racemosa*; different cores). Linear regression analyses were performed on SPSS 13 to test if there were significant correlations between two parameters (e.g., salinity and isotopic composition of biomarkers) and $p < 0.05$ is regarded as significant.

3. RESULTS

3.1. Taraxerol concentrations and carbon and hydrogen isotopic signatures in leaves of *R. mangle* and *L. racemosa* along a salinity gradient

The taraxerol concentrations in the leaves of *R. mangle* and *L. racemosa* varied from 658 to 7006 μg g^{-1} dw, and 149 to 823 μg g^{-1} dw, respectively. Significant positive correlations between taraxerol concentrations and surface water salinity were observed for both mangrove species (Fig. 2a; Table S1). *R. mangle* had a significantly higher ($p < 0.01$) averaged concentration of taraxerol than that of *L. racemosa* (Fig. S1).

The taraxerol $\delta^{13}C$ values ranged from −42.1‰ to −38.6‰, and −40.6‰ to −36.2‰ for leaves of *R. mangle* and *L. racemosa*, respectively. A significantly higher ($p < 0.01$) average taraxerol $\delta^{13}C$ value occurred in *L. racemosa* compared to *R. mangle*. A significant positive ($p < 0.01$) correlation between taraxerol $\delta^{13}C$ values and salinity was observed for *L. racemosa*, whereas the reverse trend ($p < 0.01$) was observed for *R. mangle* (Fig. 2b).

Taraxerol δ^2H values ranged from −213‰ to −171‰, and −234‰ to −188‰, respectively for leaves of *R. mangle* and *L. racemosa*. A significantly higher ($p < 0.01$) average taraxerol δ^2H value occurred in *R. mangle* compared to *L. racemosa*. The $^2H/^1H$ fractionation factors between surface water and taraxerol, $\alpha^2H_{taraxerol\text{-}sw}$, ranged from 0.7828 to 0.8342, and 0.7728 to 0.8103, respectively, for leaves of *R. mangle* and *L. racemosa*. Significant negative ($p < 0.01$) correlations between $\alpha^2H_{taraxerol\text{-}sw}$ and surface water salinity were observed for leaves of *R. mangle* (R^2 0.69) and *L. racemosa* (R^2 0.70; Fig. 2e).

The slope of the linear regressions of $\alpha^2H_{taraxerol\text{-}sw}$ relative to salinity was similar for both *R. mangle* and *L. racemosa* (Fig. 3a), but *R. mangle* had a significantly higher ($p < 0.01$) intercept than *L. racemosa* (Fig. 3d).

3.2. Taraxerol abundance and carbon and hydrogen isotopic signatures in mangrove sediment cores

The taraxerol concentrations in the sediment cores from SRE sites 2, 5, and 8 were between 32 and 662 μg g^{-1} OC, 681 to 2279 μg g^{-1} OC, and 6312 to 7980 μg g^{-1} OC, respectively (Fig. 4a, b, c). The core-averaged concentration of taraxerol was significantly higher ($p < 0.01$) in the lower

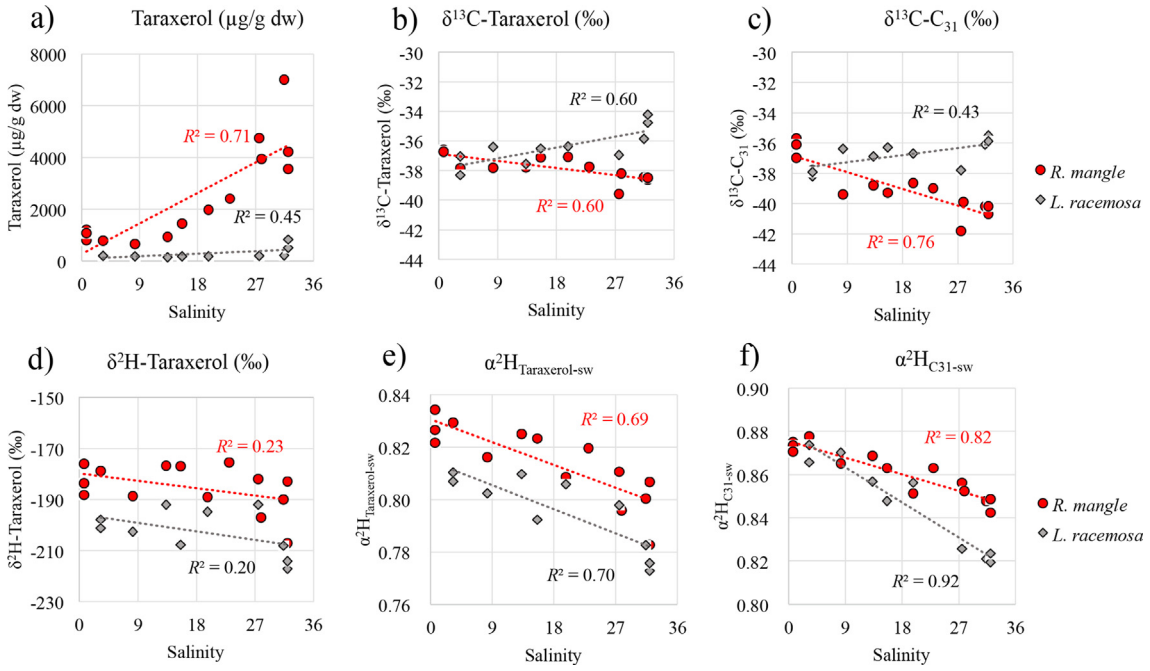

Fig. 2. The concentration and isotopic composition of taraxerol in leaf waxes of *R. mangle* and *L. racemosa* vs. surface water salinity: (a) taraxerol concentration; (b) taraxerol $\delta^{13}C$; (c) *n*-C_{31}-alkane $\delta^{13}C$; (d) taraxerol $\delta^{2}H$; (e) $\alpha^{2}H_{taraxerol\text{-}sw}$; (f) $\alpha^{2}H_{C31\ n\text{-}alkane\text{-}sw}$. The $\delta^{2}H$ and $\delta^{13}C$ values are presented on the VSMOW and VPDB scales, respectively.

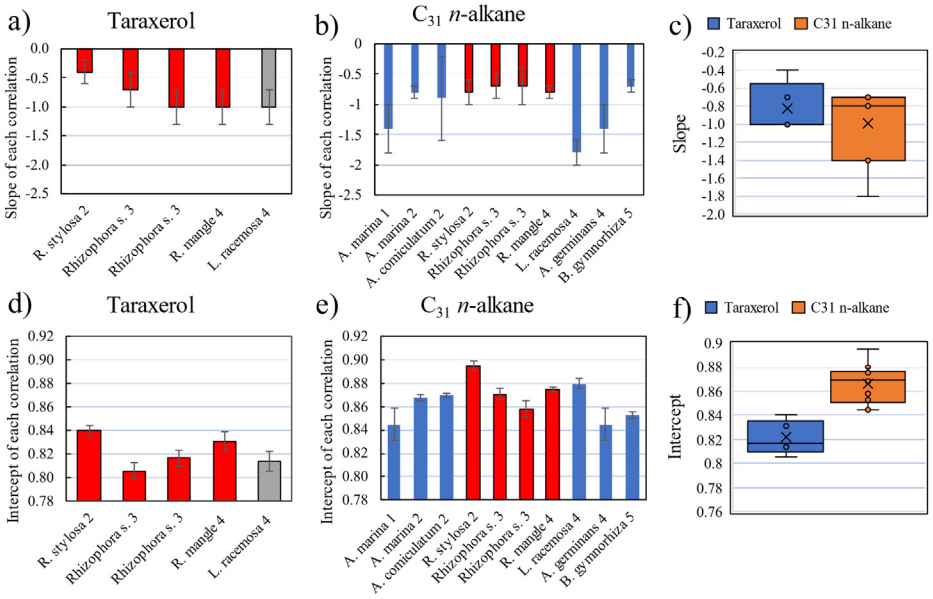

Fig. 3. Slope and y-intercept values of each linear correlation between mangrove leaf wax taraxerol or *n*-C_{31}-alkane hydrogen isotope fractionation values and surface water salinity. a) slope for taraxerol, b) slope for *n*-C_{31}-alkane, c) box whisker plot of slopes for taraxerol and *n*-C_{31}-alkane, d) intercept for taraxerol, e) intercept for *n*-C_{31}-alkane, f) box whisker plot of intercepts for taraxerol and *n*-C_{31}-alkane. Note: 1–5 denote studies from the Brisbane River estuary (Ladd and Sachs, 2012), Mobbs Bay (Ladd and Sachs, 2015a), Pohnpei estuaries (Ladd and Sachs, 2015b), SRE (this study) and Palau lakes (Ladd and Sachs, 2017), respectively. The color in panels a), b), d) and e) denotes different genus of mangroves.

estuary (site 8) than in the middle (site 5) and upper (site 2) estuary.

Taraxerol $\delta^{13}C$ values ranged from −34.8‰ to –32.6‰, −36.0‰ to –33.7‰, and −36.5‰ to −34.0‰, in cores 2, 5 and 8, respectively (Fig. 4d, e, f). Taraxerol $\delta^{13}C$ values generally increased with depth in all cores. Mean sediment $\delta^{13}C_{taraxerol}$ values decreased along the estuary, being highest at site 2 and lowest at site 8 (Fig. 5c).

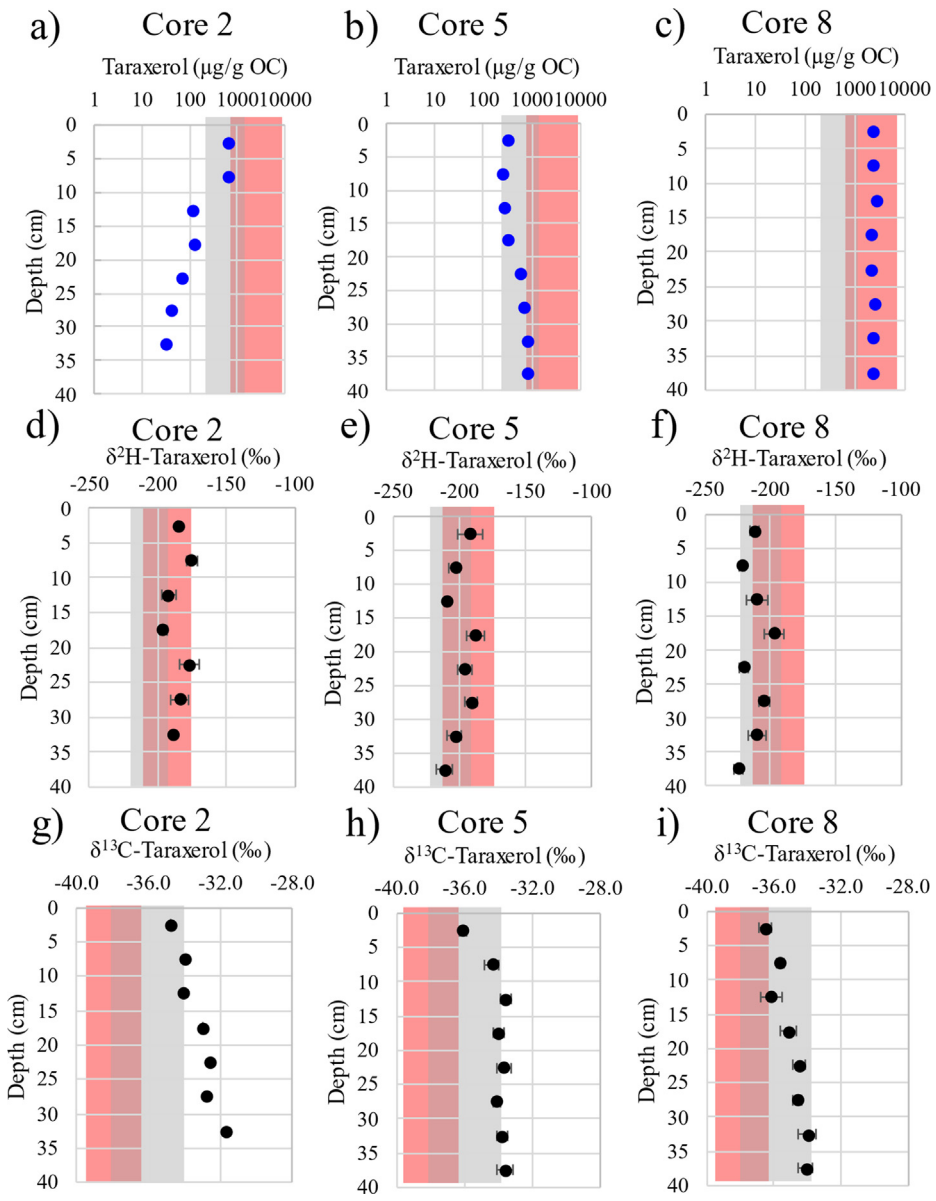

Fig. 4. The concentration and isotopic composition of taraxerol in cores 2, 5, and 8: (a-c) concentration of taraxerol; (d-f) δ^2H values of taraxerol; (g-i) $\delta^{13}C$ values of taraxerol. Note: the light red and gray area in each panel denote the range of values for *R. mangle* and *L. racemosa*, respectively. The δ^2H and $\delta^{13}C$ values are presented on the VSMOW and VPDB scales, respectively.

Taraxerol δ^2H values ranged from −196‰ to −175‰, −211‰ to −188‰, −224‰ to −197‰, in cores 2, 5 and 8, respectively (Fig. 4g, h, i). No clear trends were observed with depth in the cores, but core-mean $\delta^2H_{taraxerol}$ values decreased along the estuary, being highest at site 2 and lowest at site 8 (Fig. 5a).

3.3. Early diagenetic products of taraxerol, their abundance and carbon and hydrogen isotopic signatures in mangrove sediment cores

Based on our previous study illustrating the early diagenetic pathway of taraxerol in mangrove cores (Fig. S2; He et al., 2018b), we focus on abundances and isotopic determinations of taraxerol degradation products of a few abundant compounds such as taraxer-14-ene (**I**), des-A-taraxera-5(10),14-diene (**II**), des-A-taraxera-5(10),6,9(11), 14-tetraene (**III**), des-A-26-noroleana-5,7,9,12-tetraene (**IV**), and des-A-26,27-bisnoroleana-5,7,9,11,13,15-hexaene (**V**) (See Fig. S2 for detailed structures). Although the ring-A opening of pentacyclic triterpenoids, including taraxerol, can occur at an early diagenetic stage during leaf senescence (Jaffé et al., 1996; He et al., 2018b), the concentration of ring-A-opened intermediates of taraxerol diagenesis in leaves was too low for accurate isotopic measurements.

The concentrations and isotopic composition of compounds **I** to **V** are detailed in Table S2. Compound **I** ranged from < DL (detection limit) to 5 μg g^{-1} OC, 5 to 21 μg g^{-1}

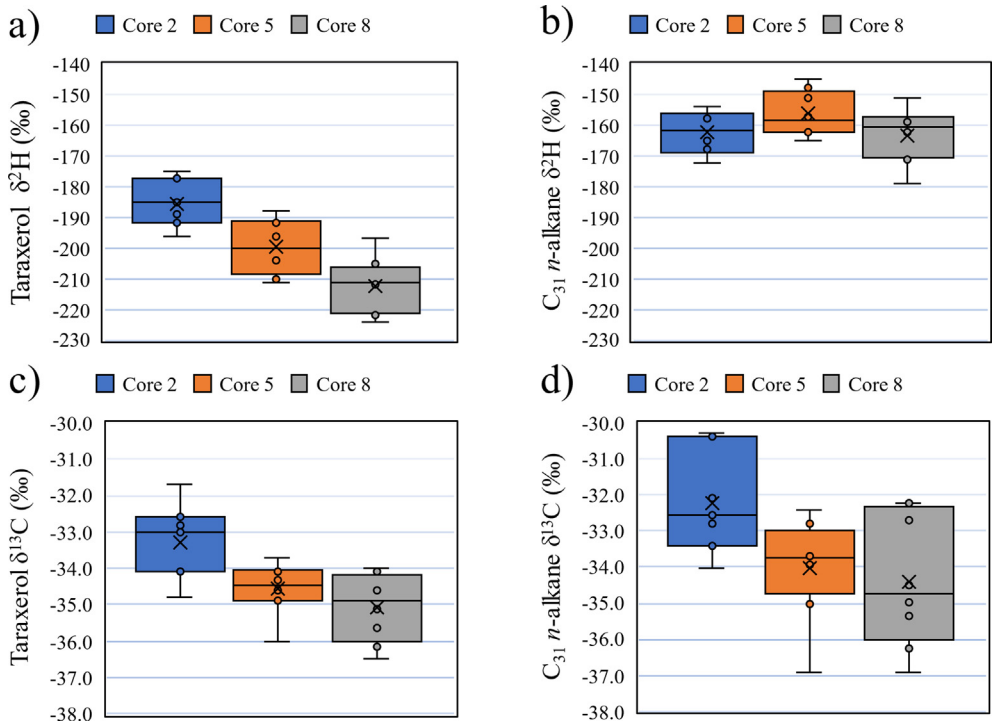

Fig. 5. The isotopic signatures of taraxerol and C_{31} *n*-alkane among cores. a) Taraxerol δ^2H values; b) *n*-C_{31}-alkane δ^2H values; c) Taraxerol $\delta^{13}C$ values; d) *n*-C_{31}-alkane $\delta^{13}C$ values. The δ^2H and $\delta^{13}C$ values are presented on the VSMOW and VPDB scales, respectively.

OC, and 5 to 14 μg g^{-1} OC, respectively, for cores 2, 5 and 8. The mean concentration of I followed the order: cores 5 > 8 > 2. The concentration of **I** showed a significant increase with depth in core 5, whereas a decreasing trend and no obvious trend with depth were observed in cores 2 and 8. **II** was the dominant diagenetic compound detected, ranging from 276 to 1377 μg g^{-1} OC, 23 to 58 μg g^{-1} OC, and 14 to 51 μg g^{-1} OC, respectively, in cores 2, 5, and 8. A significantly higher averaged concentration of **II** was observed in core 2. The concentration of **II** decreased with depth in cores 2 and 8, but increased with depth in core 5. The concentration of **III** ranged from < DL to 4 μg g^{-1} OC, <DL to 1 μg g^{-1} OC, and 5 to 24 μg g^{-1} OC, respectively, in cores 2, 5, and 8. The concentration of **III** showed a significant decrease with depth in core 8, whereas no obvious trends were observed in cores 2 and 5. Compound **IV** ranged in concentration from 1 to 80 μg g^{-1} OC, 0 to 1 μg g^{-1} OC, respectively in cores 2 and 8, but was not detected in core 5. Compound **V** ranged in concentration from 16 to 200 μg g^{-1} OC, 6 to 45 μg g^{-1} OC, respectively in cores 2 and 8, but was not detected in core 5.

$\delta^{13}C$ and δ^2H values were only obtained for taraxerol diagenetic products in a subset of the sediment samples (Table S2). The $\delta^{13}C$ values of **I** were between −34.7‰ to −34.3‰, −35.7‰ to –32.4‰, and −35.8‰ to –32.9‰ in cores 2, 5, and 8, respectively. The $\delta^{13}C$ values of **III** were between −34.3‰ to −34.0‰, and −35.9‰ to –32.8‰ in cores 2 and 8, respectively. The $\delta^{13}C$ values of **IV** ranged from −35.2‰ to –32.0‰ in core 2. The $\delta^{13}C$ values of **V** were between −35.1‰ to –33.0‰, and −35.8‰ to –32.8‰ in cores 2 and 8, respectively (Table S2; Fig. 6).

The δ^2H values of **I** were from −183‰ to −175‰, −208‰ to −182‰, and −230‰ to −199‰ in cores 2, 5, and 8, respectively. The δ^2H values of **III** were from −187‰ to −181‰, and –233‰ to −192‰ in cores 2 and 8, respectively. The δ^2H values of **IV** ranged from −201‰ to −185‰ in core 2. The δ^2H values of **V** were between −190‰ to −175‰, and −229‰ to −182‰ in cores 2 and 8, respectively (Table S2; Fig. 6).

4. DISCUSSION

4.1. Mangrove leaf taraxerol carbon isotopes and salinity

Compound-specific $\delta^{13}C$ measurements in plants are mainly focused on *n*-alkyl lipids (Pedentchouk et al., 2008; Diefendorf and Freimuth, 2017) owing to their ease of analysis. Relatively fewer studies have reported $\delta^{13}C$ values of plant terpenoids (Chikaraishi et al., 2005). Lipid biomarkers are synthesized through various biosynthetic pathways, each of which may impart a unique $^{13}C/^{12}C$ fractionation value, normally expressed as the isotopic difference between bulk leaf tissue and the lipid biomarker (Sessions et al., 1999). Triterpenoids are synthesized by the mevalonic acid (MVA) pathway of isoprenoid synthesis, which is usually 5-6‰ enriched in ^{13}C relative to *n*-alkanes that are synthesized via the acetogenic pathway (Diefendorf et al., 2012). There are very few published studies reporting $\delta^{13}C$ values for taraxerol. Lockheart et al. (1997) investigated the $\delta^{13}C$ value of taraxerol in the leaves of modern angiosperms (*Quercus robur*) and found (i) that taraxerol had lower $\delta^{13}C$ values than the C_{25} *n*-alkane, and (ii) that

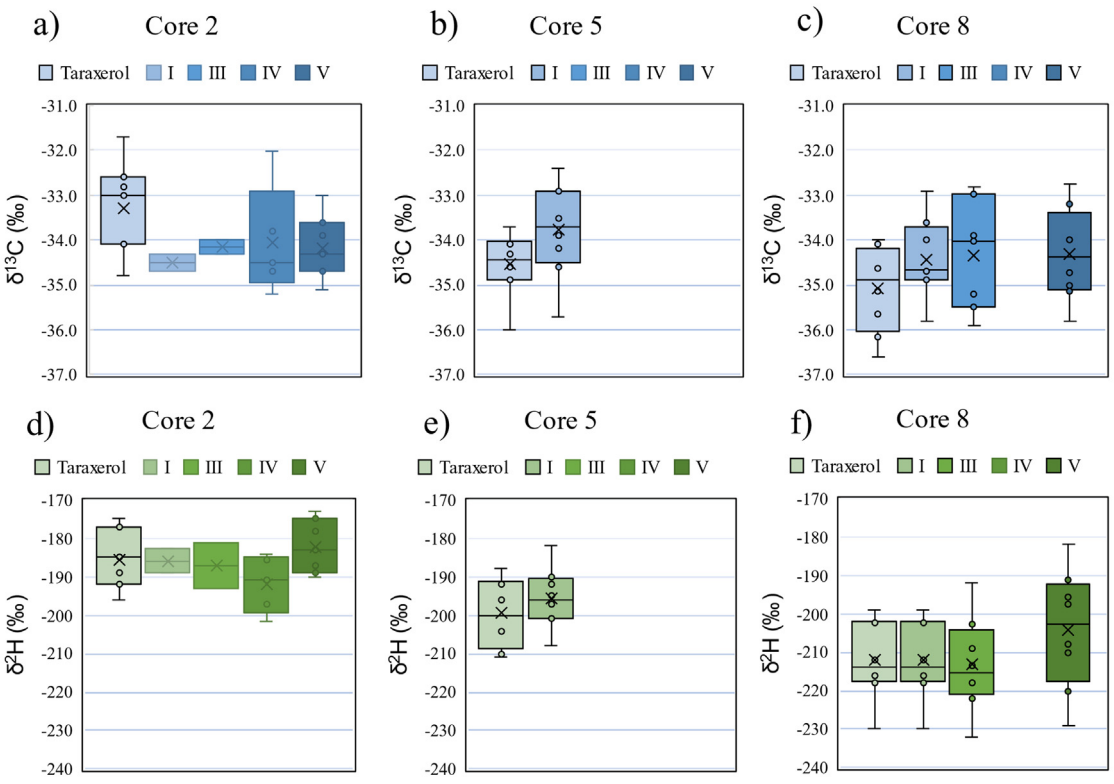

Fig. 6. Carbon and hydrogen isotopic composition of taraxerol and its diagenetic products (I, III, IV, V) at cores 2, 5 and 8. The δ^2H and $\delta^{13}C$ values are presented on the VSMOW and VPDB scales, respectively.

shaded leaves had $\delta^{13}C_{taraxerol}$ values about 4.2‰ lower than sunlit leaves, implicating light as a potential controlling variable on taraxerol $\delta^{13}C$ values.

In the SRE, the mean $\delta^{13}C$ value of taraxerol was significantly higher than that of the long-chain *n*-alkanes (e.g., *n*-C_{31}-alkane) in leaves from both *R. mangle* and *L. racemosa* (Fig. S3), consistent with previously reported greater fractionation during *n*-alkane synthesis relative to terpenoid synthesis (by ~ 1-5‰) in angiosperms (Diefendorf et al., 2012). Among other purposes, terpenoids can play defensive roles in plants, which may need to produce large quantities in a short time period, with the potential to exceed recently fixed carbon supplies. Therefore, stored carbon resources such as starch, which are typically ^{13}C-enriched relative to leaf wax *n*-alkyl lipids (e.g., Park and Epstein, 1961; Cernusak et al., 2009), can be used for synthesizing terpenoids, leading to ^{13}C-enrichment of taraxerol relative to long-chain *n*-alkanes (Diefendorf et al., 2012). The extent of ^{13}C-enrichment in taraxerol compared to long-chain *n*-alkanes is less in mangroves compared with most angiosperms, which could be caused by environmental stressors for mangroves, such as salinity gradients, that differ from those experienced by terrestrial angiosperms. However, this is beyond the scope of this study and needs further investigation.

Ladd and Sachs (2013) found a positive correlation between salinity and leaf wax *n*-alkane $\delta^{13}C$ values in *A. marina*, which was interpreted to be caused by salinity stress-induced changes in water use efficiency. This positive correlation between salinity and leaf wax *n*-alkane $\delta^{13}C$ values matched a recent study of *L. racemosa*; however, a negative correlation was observed for *R. mangle* (He et al., 2021). In the present study, the correlation between salinity and $\delta^{13}C_{taraxerol}$ is consistent with that of the *n*-C_{31}-alkane for *L. racemosa* and *R. mangle* (Fig. 2b, c). Considering *L. racemosa* and *R. mangle* were exposed to the same gradient of environmental variables, we suggest that the ecophysiological differences between *R. mangle* and *L. racemosa* likely not only affect the *n*-alkanes (synthesized by the acetogenic pathway), but also taraxerol (synthesized by the mevalonic acid pathway). In this regard, the contrasting data reflecting the effect of salinity on $^{13}C/^{12}C$ fractionation of taraxerol between *R. mangle* and *L. racemosa* potentially limits its effectiveness for paleosalinity reconstruction. Fortunately, the average abundance of taraxerol in *R. mangle* is ca. 11 times higher than that in *L. racemosa* (Fig. S1). If the vegetation coverage of *L. racemosa* is similar to or significantly lower than that of the *R. mangle*, as is the case in the SRE (Rivera-Monroy et al., 2011; Yao et al., 2015), the taraxerol detected in mangrove cores should be predominantly derived from *R. mangle*. However, in cases where such a dominance is not known, mangrove pollen could be analyzed simultaneously to better constrain the source of taraxerol and its application for paleoreconstruction in settings with mixed mangrove species (Versteegh et al., 2004; Tamalavage et al., 2020).

4.2. Mangrove leaf taraxerol hydrogen isotopes and salinity

Hydrogen isotopes of plant leaf waxes are increasingly used as a proxy for the reconstruction of past hydrologic variability (Sachse et al., 2012 and references therein). The absolute magnitude of apparent fractionation factors for taraxerol were significantly larger than those of *n*-alkyl lipids, in agreement with previous studies (e.g., Sessions et al., 1999; Sauer et al., 2001), reflecting biosynthetic control of δ^2H signatures. For instance, the averaged δ^2H values of triterpenoids were about 100‰ more depleted than those of long-chain *n*-alkanes in *Daucus carota* (Sessions et al., 1999). Here, the taraxerol δ^2H values were about 46‰-71‰ and 33‰-73‰ depleted (denoted as epsilon (ε) value as $\varepsilon^2H_{taraxerol\text{-}n\text{-}C31\text{-}alkane} = \alpha^2H_{taraxerol\text{-}n\text{-}C31\text{-}alkane} - 1$) in ^2H relative to *n*-C_{31}-alkane in *R. mangle* and *L. racemosa*, respectively (Table S1). Similar differences were observed in Micronesia (Pohnpei and Palau) (Ladd and Sachs, 2015a) and Australia (Ladd and Sachs, 2015b), where taraxerol δ^2H values were about 34‰–74‰ depleted in ^2H relative to *n*-C_{31}-alkane in *Rhizophora* mangroves (*R. stylosa*) along spatial transects and during time-series sampling. Thus, biosynthetic fractionation is likely the predominant factor causing systematic differences between *n*-C_{31}-alkane and taraxerol δ^2H values in multiple genera of mangroves in both Atlantic and Indo-Pacific regions.

A comparison of the $\alpha^2H_{lipid\text{-}sw}$ values for taraxerol and *n*-C_{31}-alkanes in SRE mangrove leaves (He et al., 2017) showed greater variability for taraxerol than for *n*-C_{31}-alkane in *R. mangle* and *L. racemosa*, implying that salinity and associated environmental factors have different apparent isotope effects in different mangrove leaf lipids.

A negative correlation between salinity and $\alpha^2H_{taraxerol\text{-}sw}$ was observed for both *L. racemosa* ($y = -0.001x + 0.8146$; $R^2 = 0.70$, $p < 0.01$) and *R. mangle* ($y = -0.001x + 0.8305$; $R^2 = 0.69$, $p < 0.01$), and no significant difference was observed in the slope of the correlation between *L. racemosa* and *R. mangle* in the SRE. This contrasts with that of the long-chain *n*-alkanes ($\alpha^2H_{C31\ n\text{-}alkane\text{-}sw}$ vs. salinity), where significantly different slopes were observed between *L. racemosa* and *R. mangle* in the SRE (He et al., 2017; Fig. 3b). When compared to published $\alpha^2H_{taraxerol\text{-}sw}$ values as a function of salinity the negative slope was indistinguishable within the uncertainty of the regressions (Ladd and Sachs, 2015a, b; Fig. 3a). In this regard, we speculate that the different $^2H/^1H$ fractionation responses to salinity between compound classes (taraxerol vs. long-chain *n*-alkanes) may arise from biosynthetic and/or biophysical differences in the production and fate of each compound, which may be synthesized at different times and/or with different internal pools of hydrogen, and/or have different turnover times within the leaf.

The taraxerol δ^2H data imply a similar sensitivity of $^2H/^1H$ fractionation to salinity in the *Rhizophora* and *Laguncularia* genera in both Atlantic and Indo-Pacific regions. Considering all available $\delta^2H_{taraxerol}$ and $\delta^2H_{C31\ n\text{-}alkane}$ data (Ladd and Sachs, 2012, 2015a, b, 2017; He et al., 2017, 2020), we speculate that taraxerol is likely a better candidate for paleoenvironmental reconstructions compared to long-chain *n*-alkanes due to its consistent response to salinity among different mangrove species, high abundance in only *Rhizophora* leaves, and high abundance in sediment records (He et al., 2018b).

4.3. Carbon and hydrogen isotopic signature of taraxerol in mangrove sediments

Several studies have demonstrated the potential of mangrove peats to store information on climatic and ecological changes (e.g., Wooller et al., 2009). Given that the stable C and H isotopic compositions of leaf wax lipids are excellent paleoenvironmental proxies (e.g., Sachse et al., 2004; Schefuß et al., 2005; Pagani et al., 2006; Aichner et al., 2010), we further test whether the hydrogen and carbon isotopic composition of mangrove taraxerol reflects the environmental gradients in the SRE. Investigation of the dual isotopic composition ($\delta^{13}C$ and δ^2H) of taraxerol might potentially provide additional and more accurate information than that obtained from less mangrove-specific biomarkers such as long-chain *n*-alkanes.

Two important factors to consider when using biomarkers for paleoreconstructions are (i) the stability of a particular compound and (ii) the isotopic fractionation (if any) during early diagenesis. Although it is difficult to directly compare the stability between long-chain *n*-alkanes and taraxerol, previous litter bag experiments suggest that taraxerol is more stable than other triterpenols (Koch et al., 2005). However, our previous study detected a variety of taraxerol diagenetic products with high concentrations in sediment cores from the SRE (He et al., 2018a). Here we investigate the extent to which diagenetic transformations affected the δ^2H and $\delta^{13}C$ values of taraxerol preserved in mangrove sediments.

We first tested whether the trends observed in leaf taraxerol were imprinted into the surface sediments. Decreases of $\delta^{13}C_{taraxerol}$ and $\delta^2H_{taraxerol}$ values were observed in surface sediments from the upper to the lower estuary (sites 2 to 5 to 8 in the SRE transect; Table S2; Fig. 5a, c). Some studies report that higher molecular-weight compounds such as long-chain *n*-alkanes are isotopically stable during early diagenesis (Huang et al., 1997; Mazeas et al., 2002), unlike lower molecular-weight compounds, such as phenol, that can display more significant isotopic fractionation during biodegradation (e.g., Hall et al., 1999). In contrast, several studies report that $\delta^{13}C$ values of long-chain *n*-alkanes in soils were usually higher by several per mil than in leaves of the dominant higher plants (Ficken et al., 1998; Lichtfouse et al., 1995; Nguyen Tu et al., 2004). For instance, Nguyen Tu et al. (2004) reported the ^{13}C-enrichment (~3‰) of long-chain *n*-alkanes from living to fallen leaves and suggested that the $\delta^{13}C$ variation might be sensitive to early diagenesis. A 1 y litter decomposition experiment for four types of grass (three C_4 species and one C_3 species) observed up to 1.7‰ ^{13}C-enrichment for long-chain *n*-alkanes (Wang et al., 2014). In addition, open plant–soil systems usually had a significant enrichment of ^{13}C for long-chain *n*-alkanes from raw leaves to soil (e.g., Chikaraishi and

Naraoka, 2006). However, most studies usually assume that long-chain *n*-alkanes in sediments or soils are predominantly derived from leaf waxes, which may not always be the case (He et al., 2020), because long-chain *n*-alkanes could also be derived from microbial inputs and aerosol deposition (Li et al., 2018; Nelson et al., 2018; Chen et al., 2021). A comparison of the C and H isotopic compositions of taraxerol and *n*-C_{31}-alkane in surface sediments from the SRE indicates that taraxerol δ^2H values are usually more depleted in ^2H but enriched in ^{13}C than that of the *n*-C_{31}-alkane in the same samples (Tables S1 and S2). This difference may be caused by (i) different turnover times of taraxerol and *n*-alkanes in mangrove leaves (e.g., leaf wax *n*-alkanes may be synthesized at leaf flush and have a longer turnover time than taraxerol (Kahmen et al., 2011)), and (ii) early diagenetic alteration of taraxerol that might alter its C and/or H isotopic composition. However, our current data cannot differentiate between these two mechanisms. Through comparing the δ^2H (and $\delta^{13}C$) differences between *n*-C_{31}-alkane and taraxerol in mangrove leaves and sediments (denoted as epsilon (ε) value as $\varepsilon = \alpha - 1$; $\varepsilon^{13}C_{\text{taraxerol-}n\text{-C31-alkane}}$ and $\varepsilon^{2}H_{\text{taraxerol-}n\text{-C31-alkane}}$, respectively), we aim to determine whether and by how much this quantity differs (Fig. S4). The results showed an obvious difference in $\varepsilon^{13}C_{\text{taraxerol-}n\text{-C31-alkane}}$ between mangrove leaves and sediments. In contrast, no significant difference in $\varepsilon^{2}H_{\text{taraxerol-}n\text{-C31-alkane}}$ was observed between mangrove leaves and cores 5 and 8, except for the lowest $\varepsilon^{2}H_{\text{taraxerol-}n\text{-C31-alkane}}$ values for the core 2. Therefore, these differences likely suggest diagenetic alteration of either the taraxerol or *n*-C_{31}-alkane isotope values, or contribution of *n*-C_{31}-alkane to sediments from non-taraxerol-producing sources (e.g., upstream freshwater wetland plants of the Everglades; He et al., 2020). In addition, further studies need to investigate the isotopic signature of taraxerol and *n*-C_{31}-alkane throughout a growing season for both *R. mangle* and *L. racemosa* at the SRE. Nevertheless, the trend observed in surface sediments is consistent with the leaf calibrations.

Triterpenoids are known to undergo diagenetic alteration processes, such as aromatization, which affects the structure of their carbon skeleton and results in the loss of carbon, oxygen and hydrogen atoms (e.g., Simoneit et al., 1986; Wolff et al., 1989; Stout, 1992; Milbeau et al., 2010; Nakamura et al., 2010; He et al., 2018b). In a previous study at the SRE, we found that the diagenetic alteration of taraxerol is mainly related to A-ring opening, further cleavage of methyl-substituted groups, and aromatization from B-ring to E-ring (He et al., 2018b). Cleavage of several C-C and C-H bonds might be associated with carbon and hydrogen isotopic fractionation. A few studies have dealt specifically with the impact of early diagenetic processes on the carbon (Freeman et al., 1994) or carbon and hydrogen isotopic compositions of sedimentary triterpenoids (Jacob et al., 2011). The main impediment to determining whether there is significant isotopic fractionation during the aromatization process is that a given aromatized terpenoid within a sediment sample can originate from mixed plant sources, each with different initial isotopic compositions. Assuming taraxerol in estuarine or marine sediments is predominantly derived from mangroves (Killops and Frewin, 1994; Versteegh et al., 2004), our work confirmed taraxerol was only found in leaves of *R. mangle* and *L. racemosa* and not in substantial amounts in other wetland plants of the Florida Everglades (He et al., 2015a, b; 2016a, b; 2018a). This source-specific origin of taraxerol is an important advantage in evaluating whether diagenesis leads to significant isotopic fractionation. Although sea level rise has had some impact on mangrove environments in South Florida, hydroclimate change at the time scale of this study has not been significant, as partially supported by paleo-palynological studies at sites 2, 5 and 8 throughout the Holocene (Yao et al., 2015; Qiang and Liu, 2017). Therefore, sites 2, 5, and 8 may serve as a potential target to test if diagenesis might lead to dramatic changes in isotopic values of taraxerol at the centennial time scale.

Comparisons of $\delta^2H_{\text{taraxerol}}$ values with depth and between core sites (2, 5, and 8) show no compelling evidence for substantial $^2H/^1H$ fractionation associated with early diagenesis (Fig. 4). No systematic $\delta^2H_{\text{taraxerol}}$ trends are observed with depth, partially supporting the assumption that diagenetic reactions on centennial timescales do not significantly influence sedimentary $\delta^2H_{\text{taraxerol}}$ values. Meanwhile, a general increase of $\delta^{13}C$ with depth was observed in all cores (Fig. 4). Up to 2‰ of the down-core ^{13}C-enrichment may be partially explained by the more enriched pre-industrial atmospheric CO_2 values compared to modern values owing to the Suess effect (Francey et al., 2002). The Suess effect alone likely accounts for part of the down-core ^{13}C-enrichment up to 3.1‰ for taraxerol. Another possibility is the directional change in plant type/composition may also shift leaf lipid $\delta^{13}C$ values over the timescale represented by these sediment cores. In this regard, Yao et al. (2015) and Yao and Liu (2017) found that mangroves are always the dominant plant species, and (ii) the pollen concentration is dominant for *R. mangle* compared with *L. racemosa* over the timespan of the sediments. Therefore, shift in mangrove species between *R. mangle* and *L. racemosa* seems less likely to account for the down-core ^{13}C-enrichment for taraxerol, and a slight ^{13}C-enrichment of taraxerol due to early diagenesis at the centennial time scale is speculated. The limited ^{13}C-enrichment (up to 3.1‰, including the 2‰ by the Suess effect) of taraxerol is in sharp contrast with that of the *n*-C_{31}-alkane, which had a $\delta^{13}C$ increase with depth up to 4.7‰. The larger down-core ^{13}C-enrichment for *n*-C_{31}-alkane compared to taraxerol suggests (i) additional sources of *n*-C_{31}-alkane other than mangroves; or (ii) diagenetic ^{13}C-enrichment of *n*-C_{31}-alkane that exceeds that of taraxerol in sediments. Considering the lack of a significant decrease of *n*-C_{31}-alkane concentration with depth (Table S2), additional sources of *n*-C_{31}-alkane other than mangroves and with different $\delta^{13}C$ value is a more likely possibility.

A previous study in the SRE identified a series of diagenetic hydrocarbons, including compounds **I** to **V**, sourced directly from taraxerol of mangroves (He et al., 2018b). Considering the detection of significantly more abundant compounds **I** to **V** and a higher average ratio of (I + II +

III + IV + V)/taraxerol in core 2 than in cores 5 and 8 (Table S2), we inferred that taraxerol underwent the most extensive degradation at site 2, followed by sites 5 and 8. This could be caused by several physiochemical factors (including salinity, microbial community composition, and nutrient concentrations) among sites and warrants further investigation. Therefore, these three cores provide an opportunity to evaluate if the differing extent of taraxerol diagenesis affected its isotopic composition.

Since the cleavage of the A-ring is a common step during the early diagenesis of taraxerol (He et al., 2018b), we compared the isotopic values between taraxerol and the des-A-triterpenes sourced from taraxerol to test whether this process significantly affected taraxerol $\delta^{13}C$ and $\delta^{2}H$ values in the SRE. Berdagué et al. (2016) has highlighted that the hydrogen isotopic composition at the various sites of the triterpenoid skeletons could be very different (up to ~ 500‰). In particular, the hydrogen atoms located on the various methyl groups in miliacin (a methoxytriterpene abundant in broomcorn millet) do not have the same isotopic composition as those bound to carbon atoms forming the benzyl ring (Berdagué et al., 2016). In contrast, some studies suggested that high molecular-weight compounds are isotopically unchangeable during biodegradation (e.g., Huang et al., 1997; Mazeas et al., 2002). However, Sun et al. (2004) found that different biomarkers exhibited distinct patterns of carbon isotopic fractionation during biodegradation experiments, with ^{13}C-enrichment of 2‰ to 7‰ for *n*-alkanoic acids, ^{13}C-depletion of 4‰ to 6‰ for alkenones and no change for sterols after 40 to 90% degradative loss of the compounds. In another study, four steroidal hydrocarbons were measured in cores from a marine bay, including cholest-2-ene, cholesta-3,5-diene, a C_{27} aromatic sterene, and a C_{28} sterene, which all showed higher $\delta^{2}H$ values by ~ 40‰ relative to their corresponding sterols, suggesting the diagenetic dehydration process may lead to ^{2}H enrichment (Li et al., 2009). However, no significant differences in $\delta^{13}C$ and $\delta^{2}H$ values were observed between taraxerol and des-A-triterpenes among our cores (Fig. 6), suggesting that the A-ring cleavage and removal of a methyl group at the C-4 location likely does not significantly affect the isotopic composition. If this is true and considering the wide detection of des-A-triterpenes in a variety of geological settings (e.g., Trendel et al., 1989; Logan and Eglinton, 1994; Otto et al., 2005; Mille et al., 2006; Huang et al., 2008; He et al., 2018b and references therein), the isotopic composition of des-A-triterpenes could have a high potential for paleoreconstructions. For instance, Bree et al. (2016) applied the carbon isotopes of des-A-lupane as an independent proxy for the time-variable carbon isotopic composition of local terrestrial C_3 plants.

4.4. Limitations and implications for paleoclimatic reconstructions using mangrove biomarkers

Reports of $\delta^{2}H$ values of taraxerol in estuarine and marine systems have been limited. Recently Nelson and Sachs (2016) demonstrated its utility to reconstruct both paleosalinity and precipitation during the Holocene when taraxerol $\delta^{2}H$ values were paired with those of dinosterol. Nevertheless, considerable uncertainties potentially leading to error propagation remained, including applying the wide range of calibration slope ratios obtained to extrapolate from *n*-alkanes to taraxerol. In particular, the net fractionation factor for ^{2}H between mangrove leaf lipids and source water decreases with salinity for *n*-C_{31}-alkane (0.7–1.8‰) in diverse genera of mangroves (*Avicennia*, *Rhizophora*, *Bruguiera*, *Laguncularia*) in tropical and subtropical estuaries and lakes from the western Pacific and Florida (Ladd and Sachs, 2012, 2015a, b, 2017; He et al., 2017). Based on this study and previous studies (Ladd and Sachs, 2015a, b, 2017), we observed a smaller range of slopes of 0.7–1.0‰ for taraxerol in both SRE (subtropical) and Micronesia (tropical) *Rhizophora* species, except for the lowest slope of 0.4‰ observed for *R. stylosa* based on a time series sampling at Mobbs Bay, Australia (Fig. 3a), which is different from other spatial sampling studies. Therefore, if past salinity and water hydrogen isotopes were to be reconstructed using $\delta^{2}H_{lipid}$ values, the salinity effect could be more confidently assessed if lipids were specifically derived from mangroves (taraxerol in this case). In this regard, this study is the second (following Nelson and Sachs, 2016) that explores the $\delta^{2}H$ of taraxerol in a natural sedimentary system, and the first to use the $\delta^{13}C$ values of taraxerol. Although non-consistent correlations were observed for taraxerol $\delta^{13}C$ values vs. salinity between *R. mangle* and *L. racemosa*, the significantly higher averaged concentration (ca. 11 times than that of *L. racemosa*) of taraxerol in *R. mangle* is likely to be the dominant factor controlling the taraxerol $\delta^{13}C$ signature in the sediments.

There are still some unconstrained factors and limitations noted as follows, which warrant further efforts to move forward with the use of sedimentary taraxerol and its stable isotopes in paleoenvironmental reconstructions. Firstly, we still have a limited understanding of which period of the isotopic signal is mostly recorded in surface sediments of mangrove habitats. Studies aimed at constraining the potential effects of the timing of leaf lipid synthesis and leaf residence time, would be helpful. Secondly, it is known that underground productivity is significant for mangroves with flourishing rootlets (Castañeda-Moya et al., 2011). With increasing salinity, mangroves increase root mass to obtain water; therefore, they are expected to have higher dry root mass under high salt stress (Castañeda-Moya et al., 2011). Root-derived organic carbon (and accompanied lipids) represents a significant source of soil organic matter (Jansen and Wiesenberg, 2017), which has been observed for the *n*-alkane series in the Everglades (He et al., 2020). However, the concentration and isotopic signature of taraxerol in the roots of *R. mangle* are unexplored. Thirdly, whether and to what extent the isotopic signals of taraxerol remain stable at the millennial (i.e., Nelson and Sachs, 2016) and longer time scales are not constrained.

We, therefore, propose the following suggestions to better constrain the utility of taraxerol for paleoenvironmental reconstructions. First, more isotopic composition data of mangrove-derived taraxerol in other regions are needed to better constrain its correlation with salinity and other factors such as nutrient availability (He et al., 2021).

Replication of calibration efforts in other subtropical mangrove forests (especially with the *Rhizophora* genus) remains critical to secure application of the proxy elsewhere, given the multiple environmental factors other than salinity that may affect the isotopic composition of lipid biomarkers (He et al., 2017, 2021). For instance, there is limited study of lipid biomarkers and their stable isotopes in the subtropical regions of China and Southeast Asia (Chu et al., 2020). Second, there is one pioneer study by Park et al. (2019) that analyzed the isotopic composition of fatty acids from five mangrove species cultivated in salinity treatments of 5–30 ppt for 3.5 years in a greenhouse. However, inconsistent net ^{2}H-fractionation with salinity was observed in this culture study compared with the field observation along salinity gradients in lakes and estuaries (Park et al., 2019). In particular, various less constrained factors still exist in Park et al. (2019) and need further investigation, such as temporal variability in $^{2}H/^{1}H$ of source water and leaf water, the timing of lipid production, temperature effect (Zhou et al., 2011), nutrient availability, and the use of stored carbohydrates. Therefore, additional culture experiments are needed under a range of controlled conditions to assess the effects of individual variables on C and H isotopic fractionation among mangrove species. Third, mangrove sediments are organic-rich, and thus can provide continuous, high-resolution records on millennial timescales (Nelson and Sachs, 2016). In the SRE, Yao et al. (2015) have retrieved mangrove deposits in the SRE dating back to ~ 3800 cal yr BP. Therefore, whether early diagenesis will affect the isotopic composition of taraxerol needs to be tested on longer time scales. Fourth, in addition to various factors including land-use changes and sea-level changes which can alter the freshwater-seawater balance and affect mangrove forests, vegetation shifts are usually accompanied by paleoclimatic changes, which are also likely in mangrove habitats where mixed mangrove species grow. In this regard, assessing the contribution of taraxerol from *R. mangle* to mangrove sediments is useful for paleoreconstruction. A recent study by Chu et al. (2020) estimated the OC contribution of *Rhizophora* to the total sedimentary OC pool. Taking the same approach, we calculated the ratio of taraxerol to C_{29} *n*-alkane for leaves of *R. mangle*, and cores 2, 5, and 8 (defined as T = taraxerol/C_{29} *n*-alkane, which is the same parameter in Versteegh et al. (2004)). Then we calculated $T_{sediment}/T_{R.\ mangle}$ (%) for each core, which ranged from 0.7 to 6.0%, 6.2 to 30.8%, and 34.7 to 50.4%, for cores 2, 5, and 8, respectively (Fig. S5). These ranges of values further suggest that relatively more taraxerol is contributed from *R. mangle* and better preserved at site 8 than sites 5 and 2. Considering the dynamic changes in the coverage of *Rhizophora* in a paleo-record, studies are encouraged to roughly assess the relative contribution of OC (including taraxerol) from *R. mangle* and *L. racemosa*, respectively. In this regard, analyzing multiple biomarker compounds with both carbon and hydrogen isotopic compositions (Galy et al., 2011; Häggi et al., 2016), can supply more detailed geochemical information. Although there are limitations specified above, this comprehensive investigation of hydrogen and carbon isotope systematics provides encouraging modern observational evidence of taraxerol to support its paleoclimate reconstructions.

5. CONCLUSION

We have conducted a calibration of leaf taraxerol $\delta^{2}H$ and $\delta^{13}C$ values along a salinity gradient in a mangrove-dominated sub-tropical estuary. The results provide support for the use of paired C and H isotopes in taraxerol as a paleoclimatic proxy in subtropical estuary environments. In particular, this study confirms that an inverse correlation exists between $\alpha^{2}H_{taraxerol\text{-}sw}$ and salinity in *R. mangle* and *L. racemosa*, thus validating the use of mangrove lipid $\delta^{2}H$ values as a paleosalinity and paleohydrological proxy. While an inverse correlation between $\delta^{13}C$ and salinity in *R. mangle*, and a positive correlation between $\delta^{13}C$ and salinity in *L. racemosa* were observed, considering the significantly higher concentration (~11 times higher) of taraxerol and more dominant presence of *R. mangle* than that of *L. racemosa*, the taraxerol preserved in sediments is likely to be mainly derived from *R. mangle* in SRE. Nevertheless, caution is warranted when working in geologic and modern sites where large vegetation fluctuations (e.g., from *R. mangle* to *L. racemosa*) occur. Additionally, it was shown that the isotopic information in leaf lipids was imprinted in the mangrove surface sediments. Although a high variety of diagenetic compounds of taraxerol were detected, no significant hydrogen isotope fractionation of taraxerol was observed, at least in the time scales of ~ 300 yrs. In contrast, early diagenesis may enrich ^{13}C of taraxerol by up to 1.1‰, after subtracting 2‰ from the potential Suess effect. Thus, the take-home message of this study focuses on the high potential application of taraxerol $\delta^{2}H$ values as a paleosalinity and paleohydrological proxy in sub-tropical and tropical coastal marine systems. Our study also highlights the need to better understand if the diagenetic degradation processes at longer time scales (e.g., millennia) could affect the carbon and hydrogen isotopic compositions of taraxerol differently compared to early diagenesis represented in this study.

Declaration of Competing Interest

The authors declare that they have no known competing financial interests or personal relationships that could have appeared to influence the work reported in this paper.

ACKNOWLEDGEMENTS

D.H. acknowledges support from the National Science Foundation of China (41973070) and the Southern Marine Science and Engineering Guangdong Laboratory (Guangzhou) (SMSEGL20SC02). This work was funded by the NSF through the Florida Coastal Everglades LTER program (DEB-1237517) to R.J. R.J. and D.H. acknowledge additional support through the George Barley Endowment and the Cristina Menendez Fellowship respectively. This work was supported by the National Science Foundation under Grants No. EAR-1348396 and OCE-1736222 (J.P.S.) and the National Science Foundation South Florida Water, Sustainability & Climate Grant No. 1204079 (J.M.S.). Prof. V.H. Rivera-Monroy is acknowledged for his help during the sampling.

We are also grateful to three anonymous reviewers, and the Associated Editor: Professor Aaron F Diefendorf for their constructive comments. This is contribution number #1000 from the Southeast Environmental Research Center at Florida International University.

APPENDIX A. SUPPLEMENTARY DATA

Supplementary data to this article can be found online at https://doi.org/10.1016/j.gca.2022.02.018.

REFERENCES

Aichner B., Herzschuh U., Wilkes H., Vieth A. and Böhner J. (2010) δD values of *n*-alkanes in Tibetan lake sediments and aquatic macrophytes-A surface sediment study and application to a 16 Ka record from Lake Koucha. *Org. Geochem.* **41**, 779–790.

Alongi D. M. and Mukhopadhyay S. K. (2015) Contribution of mangroves to coastal carbon cycling in low latitude seas. *Agr. Forest Meteorol.* **213**, 266–272.

Berdagué P., Lesot P., Jacob J., Terwilliger V. J. and Le Milbeau C. (2016) Contribution of NAD 2D-NMR in liquid crystals to the determination of hydrogen isotope profile of methyl groups in miliacin. *Geochim. Cosmochim. Ac* **173**, 337–351.

Bianchi T. S. and Canuel E. A. (2011) *Chemical biomarkers in aquatic ecosystems*. Princeton University Press.

Bree L. G. J., Rijpstra W. I. C., Al-Dhabi N. A., Verschuren D., Damsté J. S. S. and Leeuw J. W. D. (2016) Des-A-lupane in an East African lake sedimentary record as a new proxy for the stable carbon isotopic composition of C_3 plants. *Org. Geochem.* **101**, 132–139.

Breithaupt J. L., Smoak J. M., Rivera-Monroy V. H., Castañeda-Moya E., Moyer R. P., Simard M. and Sanders C. J. (2017) Partitioning the relative contributions of organic matter and mineral sediment to accretion rates in carbonate platform mangrove soils. *Mar. Geol.* **390**, 170–180.

Breithaupt J. L., Smoak J. M., Smith, III, T. J. and Sanders C. J. (2014) Temporal variability of carbon and nutrient burial, sediment accretion, and mass accumulation over the past century in a carbonate platform mangrove forest of the Florida Everglades. *J. Geophys. Res-Biogeo.* **119**, 2032–2048.

Breithaupt J. L., Smoak J. M., Smith, III, T. J., Sanders C. J. and Hoare A. (2012) Mangrove organic carbon burial rates: strengthening the global budget. *Global Biogeochem.Cy.* **26**, GB3011.

Canuel E. A., Cammer S. S., McIntosh H. A. and Pondell C. R. (2012) Climate change impacts on the organic carbon cycle at the land-ocean interface. *Annu. Rev. Earth Pl. Sc.* **40**, 685–711.

Castañeda-Moya E., Twilley R. R., Rivera-Monroy V. H., Marx B. D., Coronado-Molina C. and Ewe S. M. L. (2011) Patterns of root dynamics in mangrove forests along environmental gradients in the Florida Coastal Everglades, USA. *Ecosystems* **14**, 1178–1195.

Castañeda-Moya E., Twilley R. R. and Rivera-Monroy V. H. (2013) Allocation of biomass and net primary productivity of mangrove forests along environmental gradients in the Florida Coastal Everglades, USA. *Forest Ecol. Manag.* **307**, 226–241.

Cernusak L. A., Tcherkez G., Keitel C., Cornwell W. K., Santiago L. S., Knohl A., Barbour M. M., Williams D. G., Reich P. B. and Wright I. J. (2009) Why are non-photosynthetic tissues generally ^{13}C enriched compared with leaves in C3 plants? Review and synthesis of current hypotheses. *Funct. Plant Biol.* **36**, 199–213.

Chen X., Liu X., Jia H., Jin J., Kong W. and Huang Y. (2021) Inverse hydrogen isotope fractionation indicates heterotrophic microbial production of long-chain *n*-alkyl lipids in desolate Antarctic ponds. *Geobiology* **19**, 394–404.

Chikaraishi Y. and Naraoka H. (2005) $\delta^{13}C$ and δD identification of sources of lipid biomarkers in sediments of Lake Haruna (Japan). *Geochim. Cosmochim. Ac* **69**, 3285–3297.

Chikaraishi Y. and Naraoka H. (2006) Carbon and hydrogen isotope variation of plant biomarkers in a plant–soil system. *Chem. Geol.* **231**, 190–202.

Chikaraishi Y., Yamada Y. and Naraoka H. (2005) Carbon and hydrogen isotopic compositions of sterols from riverine and marine sediments. *Limnol. Oceanogr.* **50**, 1763–1770.

Chu M., Sachs J. P., Zhang H., Ding Y., Jin G. and Zhao M. (2020) Spatiotemporal variations of organic matter sources in two mangrove-fringed estuaries in Hainan, China. *Org. Geochem.* **147**, 104066.

Diefendorf A. F., Freeman K. H. and Wing S. L. (2012) Distribution and carbon isotope patterns of diterpenoids and triterpenoids in modern temperate C3 trees and their geochemical significance. *Geochim. Cosmochim. Ac* **85**, 342–356.

Diefendorf A. F. and Freimuth E. J. (2017) Extracting the most from terrestrial plant-derived *n*-alkyl lipids and their carbon isotopes from the sedimentary record: A review. *Org. Geochem.* **103**, 1–21.

Dodd R. S., Rafii Z. A., Fromard F. and Blasco F. (1998) Evolutionary diversity among Atlantic coast mangroves. *Acta Oecol.* **19**, 323–330.

Ficken K. J., Street-Perrott F. A., Perrott R. A., Swain D. L., Olago D. O. and Eglinton G. (1998) Glacial/interglacial variations in carbon cycling revealed by molecular and isotope stratigraphy of Lake Nkunga, Mt. Kenya, East Africa. *Org Geochem.* **29**, 1701–1719.

Francey R. J., Allison C. E., Etheridge D. M., Trudinger C. M., Enting I. G., Leuenberger M., Langenfelds R. L., Michel E. and Steele L. P. (2002) A 1000-year high precision record of $\delta^{13}C$ in atmospheric CO_2. *Tellus B* **51**, 170–193.

Freeman K. H., Boreham C. J., Summons R. E. and Hayes J. M. (1994) The effect of aromatization on the isotopic compositions of hydrocarbons during early diagenesis. *Org. Geochem.* **21**, 1037–1049.

Galy V., Eglinton T., France-Lanord C. and Sylva S. (2011) The provenance of vegetation and environmental signatures encoded in vascular plant biomarkers carried by the Ganges-Brahmaputra rivers. *Earth Planet. Sc. Lett.* **304**, 1–12.

Giri C., Ochieng E., Tieszen L. L., Zhu Z., Singh A., Loveland T., Masek J. and Duke N. (2011) Status and distribution of mangrove forests of the world using earth observation satellite data. *Global Ecol. Biogeogr.* **20**, 154–159.

Häggi C., Sawakuchi A. O., Chiessi C. M., Mulitza S., Mollenhauer G., Sawakuchi H. O., Baker P. A., Zabel M. and Schefuß E. (2016) Origin, transport and deposition of leaf-wax biomarkers in the Amazon Basin and the adjacent Atlantic. *Geochim. Cosmochim. Ac* **192**, 149–165.

Hall J. A., Kalin R. M., Larkin M. J., Allen C. C. R. and Harper D. B. (1999) Variation in stable carbon isotope fractionation during aerobic degradation of phenol and benzoate by contaminant degrading bacteria. *Org. Geochem.* **30**, 801–811.

He D., Anderson W. T. and Jaffé R. (2016a) Compound specific δD and $\delta^{13}C$ analyses as a tool for the assessment of hydrological change in a subtropical wetland. *Aquat. Sci.*, 1–14.

He D., Ladd S. N., Sachs J. P. and Jaffé R. (2017) Inverse relationship between salinity and $^{2}H/^{1}H$ fractionation in leaf wax n-alkanes from Florida mangroves. *Org. Geochem.* **110**, 1–12.

He D., Ladd S. N., Saunders C. J., Mead R. N. and Jaffé R. (2020) Distribution of *n*-alkanes and their δ^2H and $\delta^{13}C$ values in typical plants along a terrestrial-coastal-oceanic gradient. *Geochim. Cosmochim. Ac* **281**, 31–52.

He D., Mead R. N., Belicka L., Pisani O. and Jaffé R. (2014) Assessing source contributions to particulate organic matter in a subtropical estuary: a biomarker approach. *Org. Geochem.* **75**, 129–139.

He D., Rivera-Monroy V. H., Jaffé R. and Zhao X. (2021) Mangrove leaf species-specific isotopic signatures along a salinity and phosphorus soil fertility gradients in a subtropical estuary. *Estuar Coast Shelf S.* **248** 106768.

He D., Simoneit B. R. T., Xu Y. and Jaffé R. (2016b) Occurrence of unsaturated C_{25} highly branched isoprenoids (HBIs) in a freshwater wetland. *Org Geochem.* **93**, 59–67.

He D., Simoneit B. R. T. and Jaffé R. (2018a) Environmental controlling factors for the distributions of *Botryococcus braunii* (A, B and L) biomarkers in a subtropical freshwater wetland. *Sci. Rep.* **8**, 8626.

He D., Simoneit B. R. T., Cloutier J. B. and Jaffé R. (2018b) Early diagenesis of triterpenoids derived from mangroves in a subtropical estuary. *Org. Geochem.* **125**, 196–211.

He D., Simoneit B. R. T., Jara B. and Jaffé R. (2015a) Identification of a series of long-chain alkyl hydroxycinnamates from two species of cattail (*Typha domingensis* and *Typha latifolia*). *Phytochem. Lett.* **13**, 91–98.

He D., Simoneit B. R. T., Jara B. and Jaffé R. (2015b) Occurrence and distribution of a series of mono methylalkanes in the freshwater wetland of the Florida Everglades. *Chemosphere* **119**, 258–266.

Hernes P. J., Benner R., Cowie G. L., Goñi M. A., Bergamaschi B. A. and Hedges J. I. (2001) Tannin diagenesis in mangrove leaves from a tropical estuary: a novel molecular approach. *Geochim. Cosmochim. Ac* **65**, 3109–3122.

Huang X., Xie S., Zhang C. L., Jiao D., Huang J., Yu J., Jin F. and Gu Y. (2008) Distribution of aliphatic des-A-triterpenoids in the Dajiuhu peat deposit, southern China. *Org. Geochem.* **39**, 1765–1771.

Huang Y., Eglinton G., Ineson P., Latter P. M., Bol R. and Harkness D. D. (1997) Absence of carbon isotope fractionation of individual *n*-alkanes in a 23-year field decomposition experiment with *Calluna vulgaris*. *Org. Geochem.* **26**, 497–501.

Jacob J., LeMilbeau C., Bossard N., Disnar J. R. and Billaud Y. (2011) September). Combined $\delta^{13}C$-δD analysis of pentacyclic triterpenes and their derivatives. In *The 25th International Meeting on Organic Geochemistry*, p. 2p.

Jaffé R., Elismé T. and Cabrera A. C. (1996) Organic geochemistry of seasonally flooded rainforest soils: Molecular composition and early diagenesis of lipid components. *Org. Geochem.* **25**, 9–17.

Jansen B. and Wiesenberg G. L. (2017) Opportunities and limitations related to the application of plant-derived lipid molecular proxies in soil science. *Soil* **3**, 211–234.

Jennerjahn T. C. and Ittekkot V. (2002) Relevance of mangroves for the production and deposition of organic matter along tropical continental margins. *Naturwissenschaften* **89**, 23–30.

Jetter R., Kunst L. and Samuels A. L. (2006) *Biology of the Plant Cuticle*. Blackwell Publishing, UK, Oxford, pp. 145–181.

Kahmen A., Dawson T. E., Vieth A. and Sachse D. (2011) Leaf wax *n*-alkane δD values are determined early in the ontogeny of *Populus trichocarpa* leaves when grown under controlled environmental conditions. *Plant Cell Environ.* **34**, 1639–1651.

Killops S. D. and Frewin N. L. (1994) Triterpenoid diagenesis and cuticular preservation. *Org. Geochem.* **21**, 1193–1209.

Koch B. P., Harder J., Lara R. J. and Kattner G. (2005) The effect of selective microbial degradation on the composition of mangrove derived pentacyclic triterpenols in surface sediments. *Org. Geochem.* **36**, 273–285.

Koch B. P., Rullkötter J. and Lara R. J. (2003) Evaluation of triterpenols and sterols as organic matter biomarkers in a mangrove ecosystem in northern Brazil. *Wetl. Ecol. Manag.* **11**, 257–263.

Koch B. P., Souza Filho P. W., Behling H., Cohen M. C., Kattner G., Rullkötter J., Scholz-Böttcher B. and Lara R. J. (2011) Triterpenols in mangrove sediments as a proxy for organic matter derived from the red mangrove (*Rhizophora mangle*). *Org. Geochem.* **42**, 62–73.

Ladd S. N. and Sachs J. P. (2012) Inverse relationship between salinity and *n*-alkane δD values in the mangrove *Avicennia marina*. *Org. Geochem.* **48**, 25–36.

Ladd S. N. and Sachs J. P. (2013) Positive correlation between salinity and *n*-alkane $\delta^{13}C$ values in the mangrove *Avicennia marina*. *Org. Geochem.* **64**, 1–8.

Ladd S. N. and Sachs J. P. (2015a) Hydrogen isotope response to changing salinity and rainfall in Australian mangroves. *Plant Cell Environ.* **38**, 2674–2687.

Ladd S. N. and Sachs J. P. (2015b) Influence of salinity on hydrogen isotope fractionation in Rhizophora mangroves from Micronesia. *Geochim. Cosmochim. Ac.* **168**, 206–221.

Ladd S. N. and Sachs J. P. (2017) $^2H/^1H$ fractionation in lipids of the mangrove *Bruguiera gymnorhiza* increases with salinity in marine lakes of Palau. *Geochim. Cosmochim. Ac.* **204**, 300–312.

Ladygina N., Dedyukhina E. and Vainshtein M. (2006) A review on microbial synthesis of hydrocarbons. *Process Biochem.* **41**, 1001–1014.

Li C., Sessions A. L., Kinnaman F. S. and Valentine D. L. (2009) Hydrogen-isotopic variability in lipids from Santa Barbara Basin sediments. *Geochim. Cosmochim. Ac.* **73**, 4803–4823.

Li G., Li L., Tarozo R., Longo W. M., Wang K. J., Dong H. and Huang Y. (2018) Microbial production of long-chain *n*-alkanes: Implication for interpreting sedimentary leaf wax signals. *Org. Geochem.* **115**, 24–31.

Lichtfouse E., Dou S., Girardin C., Grably M., Balesdent J., Béhar F. and Vandenbroucke M. (1995) Unexpected ^{13}C-enrichment of organic components from wheat crop soils: evidence for the in-situ origin of soil organic matter. *Org. Geochem.* **23**, 865–868.

Lockheart M. J., Van Bergen P. F. and Evershed R. P. (1997) Variations in the stable carbon isotope compositions of individual lipids from the leaves of modern angiosperms: implications for the study of higher land plant-derived sedimentary organic matter. *Org. Geochem.* **26**, 137–153.

Logan G. A. and Eglinton G. (1994) Biogeochemistry of the Miocene lacustrine deposit at Clarkia, northern Idaho, USA. *Org. Geochem.* **21**, 857–870.

Mazeas L., Budzinski H. and Raymond N. (2002) Absence of stable carbon isotope fractionation of saturated and polycyclic aromatic hydrocarbons during aerobic bacterial biodegradation. *Org. Geochem.* **33**, 1259–1272.

Milbeau C. L., Schaeffer P., Connan J., Albrecht P. and Adam P. (2010) Aromatized C-2 oxygenated triterpenoids as indicators for a new transformation pathway in the environment. *Org. Lett.* **12**, 1504–1507.

Mille G., Guiliano M., Asia L., Malleret L. and Jalaluddin N. (2006) Sources of hydrocarbons in sediments of the Bay of Fort de France (Martinique). *Chemosphere* **64**, 1062–1073.

Nakamura H., Sawada K. and Takahashi M. (2010) Aliphatic and aromatic terpenoid biomarkers in Cretaceous and Paleogene angiosperm fossils from Japan. *Org. Geochem.* **41**, 975–980.

Nelson D. B., Ladd S. N., Schubert C. J. and Kahmen A. (2018) Rapid atmospheric transport and large-scale deposition of recently synthesized plant waxes. *Geochim. Cosmochim. Ac.* **222**, 599–617.

Nelson D. B. and Sachs J. P. (2016) Galápagos hydroclimate of the Common Era from paired microalgal and mangrove biomarker $^{2}H/^{1}H$ values. *P. Nat. Acad. Sci.* **113**, 3476–3481.

Newberry S. L., Kahmen A., Dennis P. and Grant A. (2015) *n*-Alkane biosynthetic hydrogen isotope fractionation is not constant throughout the growing season in the riparian tree *Salix viminalis*. *Geochim. Cosmochim. Ac.* **165**, 75–85.

Nguyen Tu T. T., Derenne S., Largeau C., Bardoux G. and Mariotti A. (2004) Diagenesis effects on specific carbon isotope composition of plant *n*-alkanes. *Org. Geochem.* **35**, 317–329.

Otto A., Simoneit B. R. T. and Rember W. C. (2005) Conifer and angiosperm biomarkers in clay sediments and fossil plants from the Miocene Clarkia Formation, Idaho, USA. *Org. Geochem.* **36**, 907–922.

Pagani M., Pedentchouk N., Huber M., Sluijs A., Schouten S., Brinkhuis H., Damsté J. J. S. and Dickens G. R. (2006) Arctic hydrology during global warming at the Palaeocene/Eocene thermal maximum. *Nature* **442**, 671–675.

Pancost R. D., Baas M., van Geel B. and Damsté J. S. S. (2002) Biomarkers as proxies for plant inputs to peats: an example from a sub-boreal ombrotrophic bog. *Org. Geochem.* **33**, 675–690.

Park J., Ladd S. N. and Sachs J. P. (2019) Hydrogen and carbon isotope responses to salinity in greenhouse-cultivated mangroves. *Org. Geochem.* **132**, 23–36.

Park R. and Epstein S. (1961) Metabolic fractionation of C_{13} & C_{12} in plants. *Plant Physiol.* **36**, 133.

Pedentchouk N., Sumner W., Tipple B. and Pagani M. (2008) $\delta^{13}C$ and δD compositions of *n*-alkanes from modern angiosperms and conifers: An experimental set up in central Washington State, USA. *Org. Geochem.* **39**, 1066–1071.

Price R. M., Swart P. K. and Willoughby H. E. (2008) Seasonal and spatial variation in the stable isotopic composition ($\delta^{18}O$ and δD) of precipitation in south Florida. *J. Hydrol.* **358**, 193–205.

Rieley G. (1994) Derivatization of organic compounds prior to gas chromatographic–combustion–isotope ratio mass spectrometric analysis: identification of isotope fractionation processes. *Analyst* **119**, 915–919.

Rivera-Monroy V. H., Twilley R. R., Davis, III, S. E., Childers D. L., Simard M., Chambers R., Jaffé R., Boyer J. N., Rudnick D. T., Zhang K., Castañeda-Moya E., Ewe S. M. L., Price R. M., Coronado-Molinag C., Ross M., Smith, III, T. J., Michot B., Meselhe E., Nuttlek W., Troxler T. G. and Noe G. B. (2011) The role of the Everglades Mangrove Ecotone Region (EMER) in regulating nutrient cycling and wetland productivity in south Florida. *Crit. Rev. Env. Sci. Tec.* **41**, 633–669.

Romero I. C. and Feakins S. J. (2011) Spatial gradients in plant leaf wax D/H across a coastal salt marsh insouthern California. *Org. Geochem.* **42**, 618–629.

Sachse D., Billault I., Bowen G. J., Chikaraishi Y., Dawson T. E., Feakins S. J., Freeman K. H., Magill C., McInerney F. A., van der Meer M. T. J., Polissar P., Robins R., Sachs J. P., Schmidt H. L., Sessions A. L., White J. W. C., West J. B. and Kahmen A. (2012) Molecular paleohydrology: interpreting the hydrogen-isotopic composition of lipid biomarkers from photosynthesizing organisms. *Annu. Rev. Earth Pl. Sc.* **40**, 221–249.

Sachse D., Radke J. and Gleixner G. (2004) Hydrogen isotope ratios of recent lacustrine sedimentary *n*-alkanes record modern climate variability. *Geochim. Cosmochim. Ac.* **68**, 4877–4889.

Sauer P. E., Eglinton T. I., Hayes J. M., Schimmelmann A. and Sessions A. L. (2001) Compound-specific D/H ratios of lipid biomarkers from sediments as a proxy for environmental and climatic conditions. *Geochim. Cosmochim. Ac.* **65**, 213–222.

Schaeffer P., Bailly L., Motsch E. and Adam P. (2019) The effects of diagenetic aromatization on the carbon and hydrogen isotopic composition of higher plant di-and triterpenoids: evidence from buried wood. *Org. Geochem.* **136**, 103889.

Schefuß E., Schouten S. and Schneider R. R. (2005) Climatic controls on central African hydrology during the past 20,000 years. *Nature* **437**, 1003–1006.

Scourse J., Marret F., Versteegh G. J., Jansen J. F., Schefuß E. and van der Plicht J. (2005) High-resolution last deglaciation record from the Congo fan reveals significance of mangrove pollen and biomarkers as indicators of shelf transgression. *Quaternary Res.* **64**, 57–69.

Sessions A. L. (2016) Factors controlling the deuterium contents of sedimentaryhydrocarbons. *Org. Geochem.* **96**, 43–64.

Sessions A. L., Burgoyne T. W., Schimmelmann A. and Hayes J. M. (1999) Fractionation of hydrogen isotopes in lipid biosynthesis. *Org. Geochem.* **30**, 1193–1200.

Sharma K. and Zafar R. (2015) Occurrence of taraxerol and taraxasterol in medicinal plants. *Pharmacognosy Rev.* **9**, 19–23.

Simoneit B. R. T., Grimalt J. O., Wang T. G., Cox R. E., Hatcher P. G. and Nissenbaum A. (1986) Cyclic terpenoids of contemporary resinous plant detritus and of fossil woods, ambers and coals. *Org. Geochem.* **10**, 877–889.

Simoneit B. R. T., Xu Y., Neto R. R., Cloutier J. B. and Jaffé R. (2009) Photochemical alteration of 3-oxygenated triterpenoids: implications for the origin of 3, 4-seco-triterpenoids in sediments. *Chemosphere* **74**, 543–550.

Smoak J. M., Breithaupt J. L., Smith, III, T. J. and Sanders C. J. (2013) Sediment accretion and organic carbon burial relative to sea-level rise and storm events in two mangrove forests in Everglades National Park. *Catena* **104**, 58–66.

Sternberg L. S. and Swart P. K. (1987) Utilization of freshwater and ocean water by coastal plants of southern Florida. *Ecology* **68**, 1898–1905.

Stout S. A. (1992) Aliphatic and aromatic triterpenoid hydrocarbons in a Tertiary angiospermous lignite. *Org. Geochem.* **18**, 51–66.

Suárez N. (2003) Leaf longevity, construction, and maintenance costs of three mangrove species under field conditions. *Photosynthetica* **41**, 373–381.

Sun M.-X., Zou L., Dai J., Ding H., Culp R. A. and Scranton M. I. (2004) Molecular carbon isotopic fractionation ofalgal lipids during decomposition in natural oxic and anoxic seawaters. *Org. Geochem.* **35**, 895–908.

Tamalavage A. E., van Hengstum P. J., Louchouarn P., Fall P. L., Donnelly J. P., Albury N. A., Coats S. and Feakins S. J. (2020) Plant wax evidence for precipitation and vegetation change from a coastal sinkhole lake in the Bahamas spanning the last 3000 years. *Org. Geochem.* **150**, 104120.

Tipple B. J., Berke M. A., Doman C. E., Khachaturyan S. and Ehleringer J. R. (2013) Leaf-wax *n*-alkanes record the plant-water environment at leaf flush. *P. Nat. Acad. Sci.* **110**, 2659–2664.

Trendel J. M., Lohmann F., Kintzinger J. P., Albrecht P., Chiarone A., Riche C., Cesario M., Guilhem J. and Pascard C. (1989) Identification of des-A-triterpenoid hydrocarbons occurring in surface sediments. *Tetrahedron* **45**, 4457–4470.

Vaughn D. R., Bianchi T. S., Shields M. R., Kenney W. F. and Osborne T. Z. (2020) Increased organic carbon burial in northern Florida mangrove-salt marsh transition zones. *Global Biogeochem. Cy.* **34**, e2019GB006334.

Versteegh G. J., Schefuß E., Dupont L., Marret F., Damsté J. S. S. and Jansen J. F. (2004) Taraxerol and Rhizophora pollen as proxies for tracking past mangrove ecosystems. *Geochim. Cosmochim. Ac.* **68**, 411–422.

Volkman J. K., Farrington J. W. and Gagosian R. B. (1987) Marine and terrigenous lipids in coastal sediments from the

Peru upwelling region at 15 °S: sterols and triterpene alcohols. *Org. Geochem.* **11**, 463–477.

Wang G., Zhang L., Zhang X., Wang Y. and Xu Y. (2014) Chemical and carbon isotopic dynamics of grass organic matter during litter decompositions: A litterbag experiment. *Org. Geochem.* **69**, 106–113.

Wanless H. R., Parkinson R. W. and Tedesco L. P. (1994) Sea level control on stability of Everglades wetlands. In *Everglades: The Ecosystem and its Restoration*. St. Lucie Press, Delray Beach, FL, USA, pp. 199–223.

Wolff G. A., Trendel J. M. and Albrecht P. (1989) Novel monoaromatic triterpenoid hydrocarbons occuring in sediments. *Tetrahedron* **45**, 6721–6728.

Wooller M. J., Behling H., Guerrero J. L., Jantz N. and Zweigert M. E. (2009) Late Holocene hydrologic and vegetation changes at Turneffe Atoll, Belize, compared with records from mainland Central America and Mexico. *Palaios* **24**, 650–656.

Xu Y. and Jaffé R. (2007) Lipid biomarkers in suspended particles from a subtropical estuary: assessment of seasonal changes in sources and transport of organic matter. *Mar. Environ. Res.* **64**, 666–678.

Xu Y., Mead R. N. and Jaffé R. (2006) A molecular marker-based assessment of sedimentary organic matter sources and distributions in Florida Bay. *Hydrobiologia* **569**, 179–192.

Xu Y., Holmes C. and Jaffé R. (2007) A lipid biomarker record of environmental change in Florida Bay over the past 150 years. *Estuar. Coast Shelf S.* **73**, 201–210.

Qiang Y. and Liu K. B. (2017) Dynamics of marsh-mangrove ecotone since the mid-Holocene: a palynological study of mangrove encroachment and sea level rise in the Shark River Estuary, Florida. *Plos One* **12**(3).

Yao Q., Liu K., Platt W. J. and Rivera-Monroya V. H. (2015) Palynological reconstruction of environmental changes in coastal wetlands of the Florida Everglades since the mid-Holocene. *Quaternary Res.* **83**, 449–458.

Zhou Y., Grice K., Chikaraishi Y., Stuart-Williams H., Farquhar G. D. and Ohkouchi N. (2011) Temperature effect on leaf water deuterium enrichment and isotopic fractionation during leaf lipid biosynthesis: results from controlled growth of C3 and C4 land plants. *Phytochemistry* **72**, 207–213.

Associate editor: Aaron F Diefendorf